


Article

# Redox flow batteries: A literature review oriented to automatic control

Alejandro Clemente <sup>1,\*</sup> and Ramon Costa-Castelló <sup>1</sup> 

<sup>1</sup> Institut de Robòtica i Informàtica Industrial, CSIC-UPC, Llorens i Artigas 4-6, 08028 Barcelona, Spain; ramon.costa@upc.edu (R.C.)

\* Correspondence: alejandro.clemente@csic.es (A.C)

Version August 15, 2020 submitted to Energies

**Abstract:** This paper presents a literature review about the concept of redox flow batteries and its automation and monitoring. Specifically, it is focused on the presentation of all-vanadium redox flow batteries which have several benefits, compared with other existing technologies and methods for energy stored purposes. The main aspects that are reviewed in this work, correspond to the characterization, modeling, supervision and control of the vanadium redox flow batteries. A research is presented where redox flow batteries are contextualized in the current energy situation, compared with other types of energy storage systems. Furthermore, a presentation about the current challenges on research, and the main existing installations is view. A discussion about the main dynamic models that have been proposed during last years, as well as the different control strategies and observers is presented.

**Keywords:** renewable sources; energy storage systems; flow battery; vanadium redox flow battery; state of charge; cell stack.

## 1. Introduction

It is well-known that we are currently living a situation of environmental crisis. This environmental crisis is linked to the need to obtain the necessary energy for society. During the last decades, most of the energy came from fossil fuels [1], that generated a large number of greenhouse gas emissions, such as CO<sub>2</sub> emissions [2,3]. For this reason, there has been a change in the energy paradigm, adopting a global transition towards more environmentally friendly activities [4].

Nowadays, the use of renewable energy sources (RES) to produce energy is growing significantly [5]. Most of these RES (wind, solar and marine) are usually discontinuous, due to their dependency on the weather conditions. This results in the difficulty, even impossibility, to schedule this type of energy sources. In order to satisfy the energy demand at times of low energy production, the need of an energy storage system (ESS) is mandatory [6,7]. ESS can store energy, normally the surplus energy from renewable sources, and provide it when the environmental conditions do not make possible to generate all the energy required. Therefore, ESS is seen as an element that can be combined with power generation systems, such as photovoltaic or wind systems [8,9]. Another important advantage apart from the load leveling, is its function as a support element for generation and distribution lines of the electricity grid [10].

There are different types of ESS depending on how energy is obtained. Mainly, it can be differentiated between mechanical, electrical and electrochemical storage systems [11]. Especially, the search for large-scale energy storage system solutions, in terms of capacity and time, has great importance due to its many benefits. During periods of RES low production, ESS can increase considerably the available power and therefore contribute to guarantee the energy supply. Table 1 summarizes the principal characteristics of the main ESS.

35 Inside the group of mechanical large-scale ESS, the most popular ones are the pumped hydro  
36 energy storage (PHES) and compressed air energy storage (CAES) systems [12]. The main advantage  
37 of PHES and CAES systems is their high energy capacity. PHES systems have also high efficiencies  
38 between 70% to 80%, claiming up to 90 % in some installations [13]. PHES systems are also the  
39 largest-capacity form of grid energy storage available, being in 2017 the type of active installations  
40 with the highest capacity with more than 184 GW worldwide, which represented 95% of all active  
41 tracked storage installations [14]. As disadvantages, both PHES and CAES require stable geological  
42 structures, which substantially limits the use of this type of systems [15]. CAES also has the drawback  
43 that its energy efficiency is less than 70% [16], even reaching values below 45% [17,18].

44 As for electric large-scale ESS, the most common is the superconducting magnetic energy storage  
45 (SMES) system [19], which is based on the use of electro-magnetic energy, and the electric double layer  
46 capacitor (EDLC) which directly uses electric energy. SMES main advantage is its energy efficiency,  
47 about 90% [20]. The main disadvantage is the high cost of superconducting wire, which, with the  
48 refrigeration energy that this system needs, makes this technology more appropriate for short-term  
49 applications [21]. The main advantages of EDLC are that can deliver large amounts of power and  
50 its long life cycle (supporting more than one million of charge and discharge cycles). On the other  
51 hand, they have low energy density, and they only can store energy for short periods of time due to  
52 the self-discharge phenomenon [22].

53 In the last group of ESS, which corresponds to the energy storage from chemical reactions, there  
54 are different batteries and emerging technologies [23]. Typical batteries that have been used for many  
55 years are Lead-Acid, Sodium-Sulphur and Lithium-Ion. The strengths of Lead-Acid batteries are their  
56 low cost and good efficiencies from 75% to 80% [24]. In counterpart, they have short life (between  
57 200 to 1800 charge and discharge cycles) and they are extremely toxic [25]. Sodium-Sulphur have  
58 higher energy density than lead-acid batteries, with similar efficiencies but with larger lifetime around  
59 2500 cycles [26,27]. The main problem of this type of technology is its operating temperature (about  
60 300°C) and a poor safety due to possible leaks of the liquids inside it. Finally, Lithium-Ion is the best  
61 choice compared to the previously named ones, having a larger energy density [28], and a long life,  
62 greater than 2500 cycles [29]. On the other hand, it is important to remark that some damages, such as  
63 overcharge or perforation cause damage to the battery, leading to explosions and fires if is damaged or  
64 incorrectly charged.

65 Nowadays, inside the group of electrochemical ESS, more research is being done, specially in fuel  
66 cells and redox flow batteries. Fuel cells [30,31] convert chemical energy from a fuel (usually hydrogen)  
67 into electric energy through an electrochemical reaction between the fuel with an oxidizing agent  
68 (oxygen). Its main distinction from a battery is that requires a continuous source of species. Combining  
69 the fuel cell with an electrolyzer it is possible to store the chemical energy, becoming an ESS, which is  
70 called regenerative fuel cell (RFC) [32,33]. One of the main advantages of its use is that is a clean ESS,  
71 being water vapor the residue that comes out. In terms of efficiency, typical values oscillate between  
72 40% to 60% [34,35]. Most losses are in the form of heat, so in the case of an application in which it is  
73 necessary to capture waste heat in a cogeneration system, efficiencies can reach 85% [36].

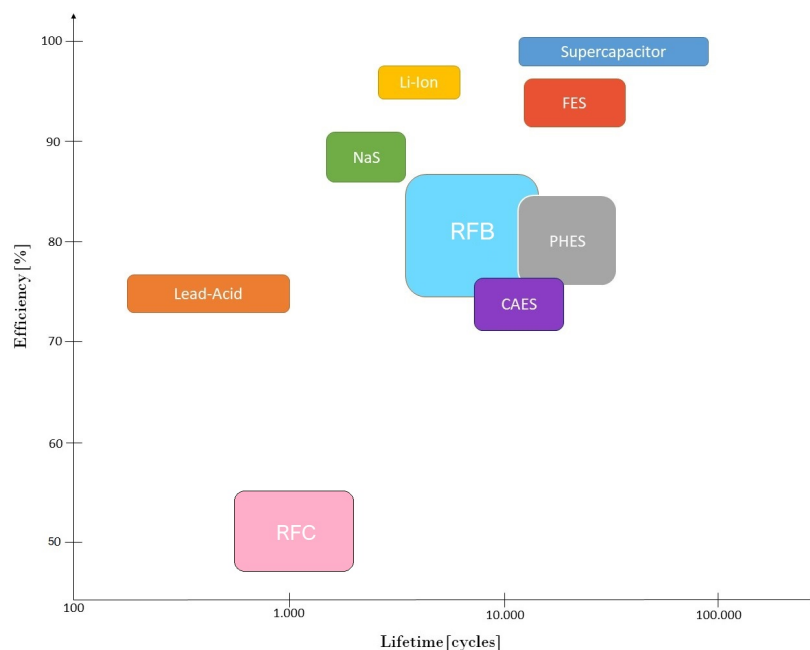
74 Redox flow batteries (RFB) are composed of an electrochemical cell where chemical energy is  
75 provided by two chemical components dissolved in liquids contained within the system and separated  
76 by a membrane. They have become one of the most promising options for large-scale energy storage  
77 systems [37,38]. Depending on the nature of the fuel, there are two modes of operation for a redox flow  
78 battery. If the flowing fuel is depleted by the reaction, and cannot be reused, then it is removed from  
79 the system and new flow is added. In this situation, it actuates as a fuel cell. The second possibility,  
80 is that it works like a rechargeable battery, where there is always fuel flowing in the system. In this  
81 second case, it is called RFB.

**Table 1.** Advantages, disadvantages, power and discharge time of main ESS. Extracted from [15].

ESS	Main Advantage	Main Disadvantage	Power	Discharge Time
PHES	High energy capacity	Geographical environment	10 MW - 1 GW	10-100 h
CAES	High energy capacity	Geographical environment	10 MW - 1 GW	1-50 h
EDLC	High power density	High cost	10 kW - 1 MW	1-10 s
Lead-Acid	Low cost	Short life cycle	1 kW - 10 MW	0.01-1 h
Sodium-sulphur	High energy	Poor safety	100 kW - 10 MW	10 h
Lithium-Ion	High energy	Poor safety	1 kW - 1MW	0.1-10 h
RFC	High energy density	Low efficiency	100 kW - 10 MW	1-10 h
RFB	Flexible design	Low energy density	100 kW - 80-90 MW	1-10 h

82 One of the main characteristics of RFB's and RFC's is the duality between energy capacity  
83 and power. Energy capacity is function of the electrolyte volume, which is usually stored in tanks.  
84 Depending on their volume, they can provide energy from minutes to several hours [39]. The power is  
85 directly related with the surface of the electrodes, and the number of cells that compose the system  
86 [40]. Other important advantages are their safety, flexible design, long life and that they are specially  
87 designed for large-scale storage applications, because self-discharge is practically non-existent, saving  
88 or providing energy during long periods of time. In terms of charge/discharge efficiency, RFB's have  
89 values between 75% to 85% [41], while RFC's have lower efficiencies. For that reason, comparing both  
90 of them, RFB's are a great proposal for large-scale ESS.

91 Comparing RFB's with other ESS, taking into account Table 1 it is possible to make clear that  
92 RFB's allow large amounts of energy to be delivered over long periods of time, without the need for a  
93 specific geographical location, as in the case of PHES and CAES systems. In terms of safety, they are  
94 better than classical batteries such as lead-acid, sodium-sulphur and lithium-ion. If they are compared  
95 in terms of efficiency and lifetime, RFB's are also a good election, as can be noticed in Figure 1.

**Figure 1.** Efficiency and lifetime comparison of main ESS. Information obtained from [42].

96 In comparison with lithium-ion batteries, which have become one of the most promising options  
97 in electrochemical ESS, VRFB have as benefits their greater lifetime, safety and low cost [43]. However,  
98 lithium-ions batteries present higher energy density. In terms of sizing, VRFB differs from lithium-ion  
99 technology in the duality between power and energy capacity. From an automatic control point of  
100 view, lithium-ion batteries contain no active elements consequently do not require any control [44]. On

101 the other hand, RFB require a good control strategy to improve its efficiency, required by the pumps  
102 which make the electrolyte flow in the system. In both technologies, obtaining good control-oriented  
103 models and developing methodologies to estimate most relevant parameters from empirical data are  
104 important research topics. Their tuning are of great relevant to estimate the State Of Charge (SOC) and  
105 the State Of Health (SOH). In the case of RFB, the SOH study has not yet been developed while for  
106 lithium-ion batteries there are already numerous studies. Although there has been a lot research in this  
107 topic it is still and open research area [45–48].

108 Analyzing the RFB individually, the main benefits of this type of ESS are [49]:

- 109 • High duration in terms of energy supply, managing to reach hours. There are several facilities in  
110 operation whose supply period is around 5 hours, although there are operational cases in which  
111 it reaches 10 hours [50].
- 112 • Modular technology, existing an independence between power and energy density. This allows  
113 to have a flexible design depending on the required operation conditions.
- 114 • Long life, higher than thousands of cycles [51].
- 115 • Thermally safe, operating at low temperatures close to ambient ones [52].
- 116 • Quickly recharge by replacing the electrolyte or reversing the redox reaction.
- 117 • Self discharge is not significant, only takes place in the cell where species react. The active  
118 species stored in the containers (which are usually much larger than the cell) do not react and  
119 self-discharge does not take place [53].
- 120 • Its operation could be stopped quickly by cutting off the flow of electrolytes.

121 Although the advantages listed above, make RFB's a good large-scale storage system, there are  
122 some drawbacks to consider. The main one is their low energy density, in comparison with other  
123 systems. In order to store large amounts of energy, it is necessary to have larger tanks. Although its  
124 charge and discharge efficiencies are high, reaching the order of 80%, is lower than other ESS, due to  
125 the energy consumption to allow the flow of electrolytes in the system.

126 There are different types of RFB's according to the species that react, but all of them present  
127 the same operating mechanism. A typical example is the Fe-Cr RFB, which uses Fe(III) and Fe(II) as  
128 positive active species, and the species Cr(III) and Cr(II) as negative ones, all of them dissolved in HCl  
129 [54]. Other examples are the iron-chromium (I-Cr) and the zinc-bromide (Zn-Br) batteries [55,56].

130 Specially, vanadium redox flow batteries (VRFB) are of great importance due to their benefits  
131 compared to other species, being the object of study in recent years [57]. The main reason for its use is  
132 that since it is made up of only vanadium, there is no possibility that different substances mix and  
133 degrade the battery. The VRFB use V(IV) and V(V) oxidation states as positive active species, and V(II)  
134 and V(III) as negative species, all of them dissolved in a solution of H<sub>2</sub>SO<sub>4</sub> [58].

135 Due to the complexity of a RFB system, that depends on different variables such as the electrolyte  
136 concentration, current density, temperature or flow management, more research will be done to  
137 understand better the RFB operation that will be directly translate in well optimized RFB systems.  
138 Moreover, due to the presence of harmful phenomena such as leakage currents, electrolyte escape  
139 and the possible corrosion and degradation of membrane, electrodes and other stack components, a  
140 research in mitigation strategies of these phenomena will be necessary [59].

141 Another important aspect to consider is the cost of the RFB system. Inside this economical  
142 scenario, more research is being done in order to design low-cost RFB systems that are capable to  
143 store large quantities of energy maximizing the performance of the battery. In order to accomplish it,  
144 the correct choice of the main components such as electrodes, membranes, bipolar plates and cells is  
145 critical. Selecting a good electrode structure allows to have a higher electrocatalytic activity, and if the  
146 surface area is higher enough, it will be possible to increase the volume production of new species.  
147 For the membrane, there are different studies that analyze and compare different materials in order  
148 to find the one that best suits with the designed battery. Thus, taking into account the species that  
149 react, as well the design of the other components, further investigations will be conducted to find an

150 equilibrium between a better selectivity and stability, as also a lower cost. In terms of bipolar plates,  
151 more research is necessary to scale-up the battery, increasing both power and energy density.

152 Considering the materials with which the RFB are built, the search for organic materials in terms of  
153 active materials, electrolytes and membranes is one of the research hot topics. In this scenario, there is  
154 recent progress in the search for organic RFB [60], which would allow to have a more environmentally  
155 attractive technology.

156 Taking into account the great possibilities that RFB's present as large-scale storage systems, as  
157 well as the numerous studies that are being carried out on them, in this work a review of most relevant  
158 concepts in RFB, from an automatic control point of view, will be presented. As previously stated  
159 other topics such as materials will be very important in the near future but are outside the scope of  
160 this work.

161 The work has the following organization: Section 2 shows the composition of a RFB; Section 3  
162 presents the main expressions needed to determine the battery sizing according to specific conditions  
163 of power and energy; Section 4 shows the main characteristics and applications of RFB; Section 5  
164 presents a review on the literature of RFB models; Section 6.1 presents the main control strategies  
165 of RFB systems, section 6.2 presents the main techniques to estimate the state of charge, and other  
166 parameters and variables. Finally, section 7 contains some conclusions and future investigations.

## 167 2. Composition and Operation of VRFB

168 RFB are secondary batteries, which means they are rechargeable. Its principle of energy conversion  
169 is based on electrochemical reactions of two redox couples [61]. As its name suggests, they are based  
170 on the principle of redox reactions. A redox reaction can be defined as a phenomenon in which there  
171 exists an exchange of electrons between two different species [62]. On the one hand, species that lose  
172 electrons are called oxidized species. On the other hand, species that win electrons are the reduced  
173 ones. The gain or loss of an electron is equivalent to a change in the oxidation state of the element.  
174 Then, both process of oxidation and reduction can be defined as:

- 175 • **Oxidation:** increased oxidation state of a specie, caused by the loss of one or more electrons.
- 176 • **Reduction:** decreased oxidation state of a specie, caused by the gain of one or more electrons.

177 Once the principles of redox reaction have been explained, it is possible to understand the operation of  
178 a redox flow battery, and their main components. Figure 2 shows the scheme of a redox flow battery  
179 with its main components.

180 A redox flow battery is composed by two electrodes whose function is to be the surface where  
181 oxidation-reduction reactions take place. The potential difference that is generated between the  
182 electrodes is determined by the electrochemical reaction that occurs, which depends on the chemical  
183 elements that make up the reaction. Lot of research has been done to find the best materials and  
184 dimensions for the electrodes. In terms of electrode composition, first investigations analyzed carbon  
185 and non-carbon materials. For the case of non-carbon materials as metals, it was found that were  
186 unsuitable for use in both half-cells [63]. Carbon has been identified as the best material for use in  
187 both electrodes of a VRFB, and different studies have been done that analyze its use and advantages  
188 [64–67].

189 The electrons that appear on the redox reaction can be defined as a current that passes through  
190 the cell continuously. Current flow exists due to the presence of two collector plates located at the end  
191 of the cell. The direction of current flow depends on whether the battery is in the process of charging  
192 or discharging. The number of electrons will depend on the current density and the electrode surface  
193 area. Typical values of current densities vary between 10 mA/cm<sup>2</sup> to 800 mA/cm<sup>2</sup>, depending on  
194 the design of the VRFB [68]. Using a Nafion membrane, usual values of current densities must vary  
195 only in a window between 80 mA/cm<sup>2</sup> to 140 mA/cm<sup>2</sup> obtaining efficiencies between 80% to 90%,  
196 because increasing the current density above the 150 mA/cm<sup>2</sup> lower efficiency is observed due to the  
197 higher ohmic resistance of Nafion membrane [69]. Different studies have analyzed the limitation of



198 the maximum current density for VRFB obtaining  $750 \text{ mA/cm}^2$  for three layers of carbon fiber paper  
199 [70]. Taking into account that typical current values vary from 20 A to 150 A it is possible to have an  
200 idea about the surface of the electrode, taking values between  $100 \text{ cm}^2$  to  $2000 \text{ cm}^2$ .

201 The main feature of this type of system is that the electrolytes are not only contained within  
202 the cell as in conventional batteries, but are stored in two independent tanks. The electrolytes are  
203 composed by the active species in a specific concentration, and are dissolved in a strong acid solution  
204 that typically is hydrochloric acid (HCl) or sulfuric acid ( $\text{H}_2\text{SO}_4$ ). One tank contains the positive  
205 electrolyte (catholyte) and the other contains the negative electrolyte (anolyte). Fluids from the tanks  
206 containing the electrolytes are pumped into two closed circuits through the battery stack (consisting of  
207 several flow cells stacked together) and the redox reaction occurs. The new species after the reaction  
208 are recirculated to their corresponding tank due to the closed circuit.

209 The electrolytes tanks always contain the same amount of liquid, but the oxidation state of each  
210 specie will depend on the reaction that takes place in the cell during the operation of the system. As  
211 long as there are species that can be transformed, the battery can continue the process of charging or  
212 discharging.

213 The membrane has the function of separating the electrolytes inside the cell, preventing them  
214 from mixing with the redox species. At the same time, it has to allow the transfer of ions to maintain  
215 the electroneutrality of the system [71]. For that reason, it is necessary to choose a special ion-selective  
216 membrane depending on the species [72]. Different types of membranes have been explored and  
217 investigated as Nafion cation exchange membranes (CEMs), tungstophosphoric acid (TPA), sulfonated  
218 polymer membranes and others [73–75]. Some studies have shown that over time, the membrane  
219 degrades and begins to appear the crossing of ions from one electrolyte to the other, polluting both  
220 electrolytes [76]. This fact causes a reduction of the efficiency and lifetime of the complete system,  
221 making it necessary to change the cell and electrolytes. Taking into account this common problem  
222 in redox flow batteries, the best solution that has been implemented in the recent years is the use of  
223 vanadium species as electrolytes [77,78]. The first VRFB's explorations were done in the 1930s, by  
224 Pissort [79]. In the 1970s, Pellegrini and Spaziante patent the VRFB [80], but they could not demonstrate  
225 the correct operation of this technology. Was Skyllas-Kazacos in the 1980s, the first person to successfully  
226 demonstrate the all-vanadium RFB [81].

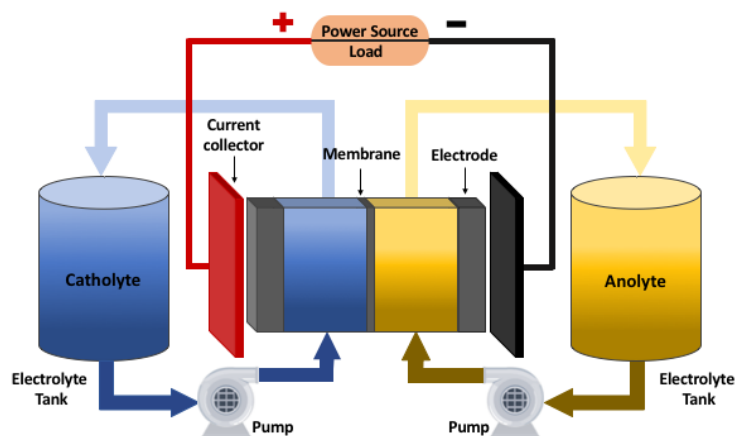


Figure 2. Scheme of a redox flow battery.

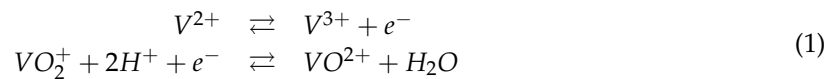
227 In a VRFB, the electrolytes contain vanadium salts dissolved in concentrated solutions of sulfuric  
228 acid. Their redox reactions involve four oxidation states of vanadium (+II, +III, +IV, +V). They are  
229 the same one with different oxidation states, allowing the possible mixing of electrolytes without  
230 becoming a problem for the system [82].

231 The negative electrolyte (anolyte) is composed by  $V^{2+}$  and  $V^{3+}$  vanadium species. The positive  
 232 electrolyte (catholyte) is composed by  $V^{4+}$  and  $V^{5+}$ . The maximum vanadium ion concentration that  
 233 can be employed for wide temperature range operation is typically 2 M or less [83,84]. This means  
 234 that for each liter of solution is composed of vanadium ions and  $H_2SO_4$ , there are 2 mols of vanadium  
 235 species dissolved on it. This concentration is equivalent to an energy density of around 25 Wh/kg.  
 236 This value ensures the solubility of vanadium ions even in temperatures below 5 °C degrees. At the  
 237 same time ensures the stability of vanadium ions at possible temperatures above 40 °C [85].

238 During the charging process, the  $V^{4+}$  oxidizes and becomes  $V^{5+}$  releasing an electron. This  
 239 electron is transferred from the anode to the cathode through external circuit, and reduces  $V^{3+}$  to  $V^{2+}$   
 240 on the other electrode.

241 During the discharging process, the oxidation of  $V^{2+}$  to  $V^{3+}$  takes place in the negative electrolyte  
 242 (anode) and the released electron goes to cathode reducing  $V^{5+}$  to  $V^{4+}$ . The vanadium species  $V^{4+}$   
 243 and  $V^{5+}$  exist as oxides, which are respectively,  $VO^{2+}$  and  $VO_2^+$ .

244 The chemical reactions that take place in the cell are the following ones:



245 where  $\rightarrow$  represents the charge process, and  $\leftarrow$  the discharge process.

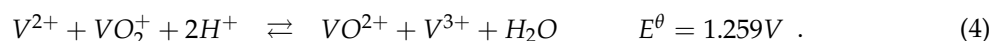
The electrochemical cell, can be seen from a chemical point of view, as a two-part system according to the presented redox equations. The cell potential has a contribution from both anode and cathode reactions. In the anode as a measure of its ability to lose electrons (oxidation potential). The cathode has a contribution based on its ability to gain electrons (reduction potential). The standard cell potential  $E^\theta$  can then be written as:

$$E^\theta = E_{cathode}^\theta - E_{anode}^\theta \quad (2)$$

The standard potential for each half-reaction process in standard conditions of pressure, concentration and temperature are defined in chemistry reaction tables [86,87]. For the case of the VRFB, the standard potential is:



Taking into account (1) and (3), it is possible to write the global reaction obtained from both reactions together, with his cell standard potential:



246 The cell standard potential gives only information about the chemical part of the reaction that  
 247 takes place inside the cell. The electrode potential  $E$  depends on the concentrations of vanadium  
 248 species  $c_i$  that exist in the cell. Its value can be obtained using (5) which is the Nernst equation:

$$E = E^\theta + \frac{RT}{F} \ln \left[ \left( \frac{c_{VO_2^+} c_{H^+}^2}{c_{VO^{2+}}} \right)_{catholyte} \cdot \left( \frac{c_{V^{2+}}}{c_{V^{3+}}} \right)_{anolyte} \right], \quad (5)$$

249 where  $R$  and  $F$  are, respectively, the gas and Faraday constant, and  $c_i$  is the concentration of each  
 250 vanadium species, which is found in the catholyte or anolyte electrolyte.

251 Taking into account equation (5) it is possible to obtain the theoretical value of the cell voltage.  
 252 As it can be noticed, it only depends on the vanadium concentrations, without any external load  
 253 connected. For that reason, it is called open-circuit voltage (OCV). It is important to take into  
 254 account, that the theoretical OCV of the VRFB has two extreme values, that correspond to a state of  
 255 complete or null charge of the cell. In both cases, these extreme values are far from those measured

256 experimentally (theoretically tend to infinity). For this reason, the extreme values of the OCV are  
 257 considered experimentally. Many studies agree that the maximum value of the cell voltage during the  
 258 charge is between 1.6 and 1.7 V, and drops to 1.1 V in the discharge case [88,89].

259 From this experimental value it is possible to see that the power that the cell can generate is not  
 260 very high. As it has been explained, VRFB's are especially useful to work with high values of power  
 261 and energy. In order to increase the power, a number of cells have to be connected in series, obtaining  
 262 what is commonly named stack. The total voltage of the stack can be calculated as the sum of all cells  
 263 voltage connected in series.

**Table 2.** Parameters and constants for Nerst Equation.

Parameter	Meaning	Unit
$c_i$	Concentration of specie i	$mol \cdot m^{-3}$
$E$	Electrode potential	V
$E^\theta$	Standard potential	V
$T$	Temperature of the cell	K
$F$	Faraday's constant	$96485 C \cdot mol^{-1}$
$R$	Gas constant	$8.314 J \cdot K^{-1} \cdot mol^{-1}$

### 264 3. Battery sizing

265 The main characteristics of VRFB's is their modularity in terms of power and energy stored. The  
 266 power directly depends on the current and stack voltage. The energy capacity depends on the volume  
 267 of the tanks. Taking into account both concepts, the objective of this section is to determine the volume  
 268 of the tanks, and the number of cells needed for the stack to guarantee any operational specifications.

#### 269 3.1. Stack Sizing

270 The power depends on the discharge/charge current and the voltage that is generated between  
 271 the electrodes of the stack. The maximum value will be reached when both current and voltage are  
 272 maximum.

The current is conditioned by the effective surface of the electrodes and the density of electric current. Assuming a constant density current ( $J$ ), the effective area of the electrode for a maximum current will be:

$$S = \frac{I_{max}}{J}. \quad (6)$$

For this maximum current, the voltage need for the stack is calculated as:

$$E_{stack} = \frac{P}{I_{max}}, \quad (7)$$

where  $P$  is the maximum amount of power that the system can generate. Then, the number of cells connected in series in the stack need to guarantee this voltage is:

$$N = \frac{E_{stack}}{E_{cell}}, \quad (8)$$

273 where  $E_{cell}$  represents the voltage that will be reached between the extremes of a cell, according  
 274 to (5). As the experimental values of cell voltage vary between 1.6 and 1.7 V [88] for the charging  
 275 operation, and between 1.0 to 1.1 during the discharge, it is a good assumption to consider that the  
 276  $E_{cell}$  value is approximately 1.1 V. With this value, it is possible to obtain a good approximation of the  
 277 number of cells that must compose the stack to obtain the desired power that the VRFB must deliver.



## 278 3.2. Tank Sizing

The energy ( $\mathcal{E}$ ) can be defined in the field of electricity as the power needed to move a charge of 1 Coulomb through a potential difference of 1 V. Then, it can be expressed as:

$$\mathcal{E} = E_{cell} \cdot Q_c, \quad (9)$$

where  $E_{cell}$  represents the potential difference, and  $Q_c$  the charge. The charge inside the tank can be calculated as follows:

$$Q_c = c_V V_{tanks} N_A e^-, \quad (10)$$

279 being  $c_V$  the total concentration of vanadium dissolved in the solution,  $V_{tanks}$  the total volume of  
280 electrolyte (vanadium species and solvent) that must be stored in the system,  $N_A$  the Avogadro constant  
281 and  $e^-$  the electron charge.

282 Taking into account that the redox reactions occur simultaneously in both half-cells, the total  
283 energy stored in  $W \cdot h$  in the system is divided between the catholyte and anolyte:

$$\mathcal{E} = \frac{1}{2} \frac{E_{cell} c_V V_{tank} N_A e^-}{3600}. \quad (11)$$

284 Finally, the necessary volume of each tank to store a required amount of energy is obtained from  
equation (11):

$$V_{tank} = \frac{7200 \cdot \mathcal{E}}{c_V E_{cell} N_A e^-}. \quad (12)$$

285

286

Table 3 summarizes all parameters that must be taken into account to design the battery sizing.

**Table 3.** Parameters for battery sizing.

Parameter	Meaning	Unit
$S$	Surface of the electrode	$m^2$
$I_{max}$	Maximum Current	A
$J$	Density of current	$A \cdot m^{-2}$
$E_{stack}$	Stack voltage	V
$E_{cell}$	Cell Voltage	V
$P$	Power	W
$N$	Number of cells	—
$\mathcal{E}$	Energy	Wh
$Q_c$	Electric charge	C
$c_V$	Total vanadium concentration	$mol \cdot m^{-3}$
$V_{tank}$	Tank volume	$m^3$
$N_A$	Avogadro constant	$6.02 \cdot 10^{23} mol^{-1}$
$e^-$	Electron charge	$1.602 \cdot 10^{-19} C$

It is important to notice that from equation (12) it is possible to derive the energy density per volume unit ( $\mathcal{E}_\rho$ ) as:

$$\mathcal{E}_\rho = \frac{\mathcal{E}}{2V_{tank}}. \quad (13)$$

287

288

289

290

291

292

293

The energy density of the complete system that makes up the VRFB is smaller than the ones calculated by (13). Theoretically, the energy density of VRFB systems is about 28 Wh/l, but in real applications it has been found that the ranges go from 15 to 25 Wh/l [90].

The difference between the theoretical energy density value and the real one found experimentally, is due to the following factors [88]:

- The pump consumes energy to make the liquid flow.

- 294 • The power converter has electrical losses, while the pipes and pumps have hydraulic losses.  
 295 • The electrochemical is subject to reaction Internal losses such as activation overpotential,  
 296 concentration overpotential and ohmic losses, which depend on the operational conditions  
 297 [91].

298 All these factors are difficult to collect in analytical models and expressions. For that reason, to  
 299 check the real effect is necessary to develop experiments or simulations with high accuracy. Therefore,  
 300 it is necessary to correctly determine the parameters of all elements, obtaining non-general results.  
 301 According to literature, the total efficiency is around an 80% of the theoretical one [92].

### 302 3.3. Example

303 In order to have a practical idea of the battery sizing of a VRFB with real values, an example is  
 304 shown. The proposed VRFB is a 1.5 kW, and 15 kWh system operating at a nominal current of 50 A.  
 305 Table 4 shows the battery parameters for this example.

**Table 4.** Battery sizing example

Parameter	Meaning	Unit
$P$	Power	1.5 kW
$\mathcal{E}$	Energy	15 kWh
$I_{max}$	Maximum Current	50 A
$E_{cell}$	Cell Voltage	1.4 V
$c_V$	Total vanadium concentration	2 M
$N$	Number of cells	27
$V_{tank}$	Tank volume	0.4 m <sup>3</sup>
$\mathcal{E}_\rho$	Energy density	18.75 Wh · l <sup>-1</sup>

306 As it can be seen in Table 4, 2 tanks of 400 liters capacity would be needed. This would represent  
 307 a total amount of approximately 732 kg of H<sub>2</sub>SO<sub>4</sub> which is the solvent, and 178 kg of vanadium species  
 308 which represent the solutes that react inside the cell, based on the molar mass of the electrolyte species  
 309 [90,93]. These amounts of chemical species have been calculated taking into account the typical value  
 310 of vanadium ion concentration, which, as explained, usually is 2 M.

## 311 4. Main existing applications and installations

312 One of the main characteristics of flow batteries is that they are considered to be used for large  
 313 energy storage applications. Taking into account its large operational range in terms of power and  
 314 energy, these systems are a good choice for all those stationary applications that require large stored  
 315 energy. Some examples are:

- 316 • Interstitial storage, due to the volume of the systems they are designed to be placed in  
 317 stationary applications that require a specific demand of power depending on factors such as the  
 318 weather, season or day, among others.  
 319 • Load leveling function, storing the surplus energy during off-peak demand periods, and using it  
 320 during periods of high demand of energy. This guarantees the existence of a balance between the  
 321 supply and the demand energy [94].  
 322 • Uninterruptible power supply (UPS) in case of failure of the main power source, being necessary  
 323 to provide power continuously for a certain period of time [95].  
 324 • Support systems in renewable energy installations, such as wind or solar, during periods of high  
 325 energy demand. Specially, in stand alone power systems where power can not be obtained from  
 326 the electric grid [96].  
 327 • Electric or hybrid vehicles, especially those of large dimensions due to its low energy density [97].  
 328 Some examples are buses and maritime vehicles such as boats, ships or submarines.  
 329 • Storage applications that require a full charge from an initial, empty state to full load. Due to the  
 330 VRFB's ability to perform full charge cycles, they are useful in this regard. A particular case are

331 solar installations where you want to be able to store as much energy as possible depending on  
332 weather conditions.

333 There are different installations that have adopted VRFB's for some of the different applications  
334 described. Table 5 lists the main existing facilities, with their respective details regarding operational  
335 characteristics and applications.

336 In 1996 the Kashima-Kita Electric Power group from Japan, develop a VRFB of 200 kW of power  
337 and 800 kWh, for load-leveling applications [98]. Kansai Electric company, has been developing  
338 RFB in collaboration with Sumitomo Electric Industries, since 1985. In 2000 they installed in Tatsumi  
339 substation a prototype of 200 kW 8 h system [99]. It was conceived for applications in load-leveling  
340 and peak-shaving. Sumitomo Electric Group from Japan, developed a 4 MW 6 MWh VRFB, in 2005,  
341 for peak-shaving and UPS applications [100]. It is one of the leading companies of RFB's, and has  
342 successfully run many pilot projects worldwide. In 2016, the Hokkaido Electric Power Company  
343 (HEPCO), developed the largest flow battery project until that moment. The installation of 15 kW 60  
344 MWh was aimed to the grid integration of wind renewable energy [101]. In Pfinztal, Germany, the  
345 Fraunhofer institute launched a project to installate a VRFB of 2kW and 20 MWh for testing purposes  
346 [102].

**Table 5.** Main existing installations of VRFB's in the world.

Name	Place	Year	Energy	Power
Kashima-Kita Electric Power [98]	Japan	1996	800 kWh	200 kW
Kansai Electric [99]	Japan	2000	1.6 MWh	200 kW
Sumitomo Electric Group [100]	Japan	2005	6 MWh	4 MW
Hokkaido Electric Power [101]	Japan	2016	60 MWh	15 kW
Fraunhofer Project [102]	Germany	2019	20 MWh	2 kW

347 It is important to notice how the amount of stored energy has been growing over the years. The  
348 Hubei Zaoyang project planned to install in Zaoyang an installation that could reach 10 MW of power  
349 and 40 MWh of energy stored [103]. This project took place in China, where a great investment in  
350 VRFB's has been launched by the China National Development and Reform Commission (NDRC) to  
351 develop different projects. Hubei Zaoyang has launched the installation of a 100 MW and 500 MWh  
352 redox flow system [104]. Another project under way is a 200 MW and 800 MWh vanadium ESS in  
353 Dalian, carried out by chinese companies UniEnergy Technologies (UET) and Rongke Power [104].

## 354 5. Mathematical models

355 To study the behaviour of the VRFB's from a theoretical point of view, it is necessary to model the  
356 real system taking into account the variables that make it up. Most of the systems use mathematical  
357 models, that can take different forms using dynamic formulation, differential equations, statistical  
358 models or logical formulation, among others. The mathematical model of a system can be based on  
359 one or more parts of study.

360 The first distinction that exists between models is how the behavior of the system is described as  
361 a function of time. That is to say, whether the effect of time is taken into account or not. If time is taken  
362 into account, the model is dynamic whereas if the system is not time dependent, it is called static [105].  
363 In terms of model VRFB's, it is obvious that due to the characteristics of both flow and current, it must  
364 be modeled taking into account the behavior along the time.

365 The second distinction for modeling is taking into account, or not, the space dimension. Models  
366 that take into account the space dimension are usually named **Distributed parameter models** and use  
367 partial derivative equations. In RFB's there exist many phenomena that can only be described through  
368 distributed models, such as the distribution of the vanadium species or temperature along the tanks  
369 and cells, or the flow rate in the pipes. There are different studies that have modeled some aspects  
370 of the RFB using this type of model [106]. These models make possible to analyze how the flow is

distributed along the cells, obtaining a realistic approximation about the distribution of vanadium concentration inside them [107]. Non-uniform distribution of flow field is analyzed using a parameter distributed model in [108,109]. One of the main computational tools that exist to obtain 3D models, is COMSOL [110], which is a finite element analysis, that allows to solve multiphysics systems. This software has been used to analyze the VRFB performance taking into account the electrode and flow field [111].

The disadvantage of **Distributed parameter models**, is that they are very complex and they can not be used for analytical analysis. Their solution requires relevant computational resources and can not be solved in short time.

For this reason, RFB automatic control problems are addressed using reduced order models, or **Lumped parameter models**. In this type of models most relevant variables, such as current or flow, do not depend on space. These assumptions allows to simplify the model. These models allow to perform analytical analysis and obtain their solution with a reduced computational cost. Despite its simplicity these models closely resemble the actual behavior of the system [112]. In this scenario, multiple and different models have been proposed.

A VRFB system, can be mainly separated in three different physical models, which are the electrochemical, the thermal and the hydraulic. All of them are interconnected. In the electrochemical part, the current and flow rate play a key role, but the temperature has also importance. In the thermal model, the concentration of species from the electrochemical part, together with the flow rate and current are the important factors to take into account. Finally, the hydraulic part is related to the other models by the flow rate, which is the variable that plays the key role. In the following, a review of the characteristics of each of these parts is presented.

### 5.1. Electrochemical model

One of the main parts of interest of the VRFB's is the behaviour of the vanadium concentrations. As have been explained, it has a direct effect on the voltage and therefore, in the power and energy of the system. There are different approaches to model the electrochemical part.

Some studies use differential equations that determine the behaviour of concentration of vanadium species through the redox reactions that take place [113,114]. Another ones, take into account the Nerst equation, and by measuring the voltage are able to model the behaviour of vanadium concentration species inside the system [115]. This second approach, has the drawback that it only takes into account the cell voltage, and not the input variables such as the flow rate or current. For this reason, it cannot be used for control purposes, since input variables such as current or flow rate, that are the only ones that the user can manage, have not effect in the model presented. Finally, there are some studies which use equivalent circuit models, to describe the behaviour of the electrochemical part. An electric circuit model is used in [116,117] to model the state of charge. Another study that uses this type of model to monitor the capacity decay of the VRFB is [118].

Using directly the redox reactions that take place, it is possible to obtain a model of the vanadium concentration variation along the time. A realistic electrochemical model was develop by Maria Kazacos [114], which is based on the determination of the vanadium concentrations behaviour with respect to the current and the flow rate of electrolytes. This model has been widely used in different studies [119–121].

The model assumes an homogeneous concentration in the cell. The behaviour of the concentrations changes in a cell ( $c_i^{cell}$ ) for RFB of any species is described by the following differential equation:

$$\frac{V_{cell}}{2} \frac{dc_i^{cell}}{dt} = Q(c_i^{tank} - c_i^{cell}) \pm \frac{I}{zF} - D_i, \quad (14)$$

where  $V_{cell}$  is the volume of the cell,  $c_i^{tank}$  is the concentration of vanadium in the tank and  $F$  the Faraday's constant. As can be noticed in equation (14) the concentration of each vanadium species,  $i$ , depends on three different factors, which are the flow rate, the current and the diffusion:

- 415 • **Q**: is the electrolyte flow rate. The amount of new electrolyte inside the cell, be understood as the  
 416 difference between the input flow of concentrations (which comes from the tanks) and the output  
 417 (the previous time concentration in the cell).
- 418 • **I**: represents the current and is directly related to the redox reaction that takes place in the cell.  
 419 The relation between the reduction or oxidation of a vanadium specie and an electron is 1/1  
 420 ( $z = 1$  for vanadium redox flow systems) as can be observed in VRFB's redox reaction (1). For a  
 421 positive current, vanadium species  $V^{2+}$  and  $V^{5+}$  increases, while  $V^{3+}$  and  $V^{4+}$  species decreases  
 422 in the cell. For discharge currents, the opposite happens. Using the Faraday's constant is possible  
 423 to establish the concentration of vanadium species in mols.
- **D<sub>i</sub>**: is the diffusion part. Depends on each vanadium specie, and is defined and modelled by Fick's law:

$$D_i = \frac{S}{d} (\alpha_{II_i} k_2 c_2^{cell} + \alpha_{III_i} k_3 c_3^{cell} + \alpha_{IV_i} k_4 c_4^{cell} + \alpha_{V_i} k_5 c_5^{cell}), \quad (15)$$

where  $S$  is the membrane surface,  $d$  the membrane thickness,  $\alpha_i$  express the mass balance between the vanadium species and  $k_i$  is the diffusion coefficient of each specie, which depends on the temperature by the following Arrhenius equation [119]:

$$k_i = A_0 e^{\frac{-E_i}{RT_{stack}}}, \quad (16)$$

424 being  $A_0$  a pre-factor,  $E_i$  the activation energy of specie  $i$ ,  $R$  the universal gas constant and  $T$  the  
 425 temperature of the electrolyte inside the stack.

426 Finally, it is possible to model the concentration of vanadium specie in a cell using the state-space  
 427 representation for the case of a charging process (positive current):

$$V_{cell} \frac{d}{dt} \begin{bmatrix} c_2^{cell} \\ c_3^{cell} \\ c_4^{cell} \\ c_5^{cell} \end{bmatrix} = \begin{bmatrix} c_2^{tank} - c_2^{cell} \\ c_3^{tank} - c_3^{cell} \\ c_4^{tank} - c_4^{cell} \\ c_5^{tank} - c_5^{cell} \end{bmatrix} Q + \frac{1}{zF} \begin{pmatrix} 1 \\ -1 \\ -1 \\ 1 \end{pmatrix} I + \frac{S}{d} \begin{pmatrix} -k_2 & 0 & -k_4 & -2k_5 \\ 0 & -k_3 & 2k_4 & 3k_5 \\ 3k_2 & 2k_3 & -k_4 & 0 \\ -2k_2 & -k_3 & 0 & -k_5 \end{pmatrix} \begin{bmatrix} c_2^{cell} \\ c_3^{cell} \\ c_4^{cell} \\ c_5^{cell} \end{bmatrix}. \quad (17)$$

In the case of a discharging process, the unique difference will be the sign of the current vector. The tanks, can be modelled taking into account the number of cells that compose the stack:

$$V_{tank} \frac{d}{dt} \begin{bmatrix} c_2^{tank} \\ c_3^{tank} \\ c_4^{tank} \\ c_5^{tank} \end{bmatrix} = N \begin{bmatrix} c_2^{cell} - c_2^{tank} \\ c_3^{cell} - c_3^{tank} \\ c_4^{cell} - c_4^{tank} \\ c_5^{cell} - c_5^{tank} \end{bmatrix} Q, \quad (18)$$

428 where  $V_{tank}$  is the volume of each electrolyte tank and  $N$  is the number of cells that compose the  
 429 stack.

430 The states of the system are the vanadium concentrations of both tanks and cells, while the other  
 431 parameters are constants or variables that can depend on the operating conditions as the temperature.

432 It is important to remark, that this mathematical model is a realistic approach of a VRFB, and  
 433 it allows to understand what factors change the vanadium concentrations inside the cell and in the  
 434 tanks. This is of great importance, since the concentrations in the cell determine the voltage, which is  
 435 calculated by Nerst expression (5), and the concentrations inside the tank determine the state of charge  
 436 (SOC) of the battery:

$$SOC = \left( \frac{c_2^{tank}}{c_2^{tank} + c_3^{tank}} \right) = \left( \frac{c_5^{tank}}{c_4^{tank} + c_5^{tank}} \right) \quad (19)$$

437 All parameters that appear are summarized in Table 6.

**Table 6.** Parameters of the electrochemical model.

Parameter	Meaning	Unit
$c_i^{cell}$	Concentration of specie $i$ ( $i=2\dots5$ ) inside the cell	$mol \cdot m^{-3}$
$c_i^{tank}$	Concentration of specie $i$ ( $i=2\dots5$ ) inside the tank	$mol \cdot m^{-3}$
$V_{cell}$	Volume of cell	$m^3$
$V_{tank}$	Volume of each tank	$m^3$
$Q$	Flow rate	$m^3 \cdot s^{-1}$
$I$	Current	$A$
$S$	Surface area of the electrode	$m^2$
$d$	Membrane thickness	$m$
$k_i$	Difussion coefficient	$m^2 \cdot s^{-1}$
$N$	Number of cells of the stack	—
$z$	Number of electrons involved in the redox reaction	1
$F$	Faraday's constant	$96485C \cdot mol^{-1}$
$R$	Gas constant	$8.314J \cdot K^{-1} \cdot mol^{-1}$

## 438 5.2. Thermal model

439 Usually, the effect of temperature on VRFB's is not detrimental to the system efficiency, since it  
 440 is normally found close to environmental values [119]. However, it has been seen that under certain  
 441 operational conditions, and depending on the membrane, there can be an increase in the temperature  
 442 above the environmental one [120]. In this situation, a heat exchanger mechanism could be necessary  
 443 to improve the behaviour of the battery. Furthermore, as the temperature is an easy variable to measure  
 444 in any physical system, obtaining a thermal model for VRFB's can help to monitor its correct operation,  
 445 or even its possible automatic control [121].

446 The correct determination of the temperature inside the stack is necessary for two main factors.  
 447 On the one hand, it can determine how much heat is absorbed or generated during the reaction [122].  
 448 On the other hand, it is directly related with the diffusion coefficients which play an important role  
 449 inside the electrochemical model.

450 Taking into account the main components of the system, which are the stack, the tanks and the  
 451 hydraulic transmission line composed by the pipes and pumps, it is possible to model the temperature  
 452 of each part as it is done on [122]. It is important to consider the external temperature of the system,  
 453 which is that of the air ( $T_{air}$ ). Figure 3 shows the different points where the temperature of the system  
 454 is modeled.

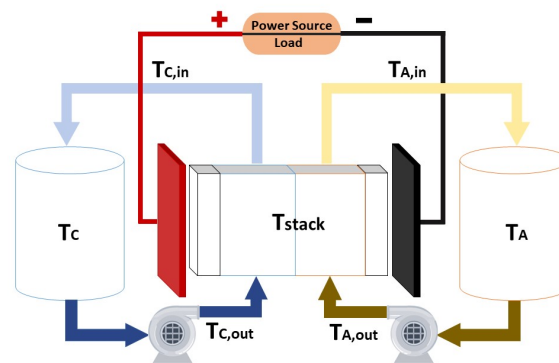


**Figure 3.** System temperature measurements.

455 The nomenclature of the subscripts of the temperature variables is summarized in Table 7.



**Table 7.** Subscripts of temperature variables.

Subscript	Meaning
C	Catholyte tank
A	Anolyte tank
C, out	Pump line of catholyte
C, in	Transmission line of catholyte
A, out	Pump line of anolyte
A, in	Transmission line of anolyte
stack	Stack of cells

The variation of the different temperatures can be model by using the energy balance equations. Equation (20) model the behaviour of the temperature in the stack [120].

$$C_p \rho V_{stack} \frac{dT_{stack}}{dt} = QC_p \rho [T_{C,out} - T_{stack}] + QC_p \rho [T_{A,out} - T_{stack}] + U_s A_s [T_{air} - T_{stack}] + N \frac{S}{d} (-k_2 \Delta H_2 - k_3 \Delta H_3 - k_4 \Delta H_4 - k_5 \Delta H_5) \cdot \begin{bmatrix} c_2^{cell} \\ c_3^{cell} \\ c_4^{cell} \\ c_5^{cell} \end{bmatrix} + I^2 r, \quad (20)$$

where  $C_p$  is the specific heat,  $\rho$  is the density of electrolyte,  $Q$  is the flow rate and  $U_s A_s$  is the heat transfer capability of the stack. The parameters  $\Delta H_2$ ,  $\Delta H_3$ ,  $\Delta H_4$  and  $\Delta H_5$  represent the change of enthalpy, which have an experimental value calculated at 298.15 K for each reaction [123]. The values of the enthalpies are negative [120] during the charging process, which yields to the conclusion that the reaction is exothermic. This means that the system releases energy in form of heat to the environment. During the discharging process, the sign of the enthalpy part in (20) changes, taking place an endothermic reaction. In (20) also appears the thermal factor due to the ohmic losses produced by the stack resistance,  $r$ , which experimentally changes its value during operation, but for practical purposes it can be assumed constant [120]. It should be noted that most of the heat generated is due to the ohmic effect, having values between few tens of Joules (currents below 50 A) to hundreds of Joules (for currents in the order of 100 A) [119].

In the tank and transmission line corresponding to the catholyte part of the system, the temperature equations are:

$$C_p \rho V_{tank} \frac{dT_C}{dt} = QC_p \rho [T_{C,in} - T_C] + U_{tank} A_{tank} [T_{air} - T_C] \quad (21)$$

$$C_p \rho V_{pipe} \frac{dT_{C,in}}{dt} = QC_p \rho [T_{stack} - T_{C,in}] + U_{pipe} A_{pipe} [T_{air} - T_{C,in}] \quad (22)$$

$$C_p \rho V_{pipe} \frac{dT_{C,out}}{dt} = QC_p \rho [T_C - T_{C,out}] + U_{pipe} A_{pipe} [T_{air} - T_{C,out}] + W_{pump} \quad (23)$$

For the case of the negative side of the system, the same equations model the behaviour of the temperature in a symmetrical way respect to Figure 3. If it is assumed that the four parts in which the pipes are divided are equals and the flow rate that circulates along the pipes is the same, then same temperatures will exist on both sides of the system. Table 8 summarizes all parameters of the thermal model.

There exist different studies done in terms of thermal parameters of RFB's. This is the case of [124], that presents a dynamic electro-thermal model. A thermal model with heat exchangers is presented in [125], proposing an effective cooling strategy.

**Table 8.** Parameters of the thermal model.

Parameter	Meaning	Unit
$C_p$	Specific heat capacity of vanadium	$J \cdot kg^{-1} \cdot K^{-1}$
$\rho$	Vanadium density	$kg \cdot m^{-3}$
$V_{stack}$	Volume of the stack	$m^3$
$V_{pipe}$	Volume of pipe	$m^3$
$Q$	Flow rate of electrolyte	$m^3 \cdot s^{-1}$
$U_s A_s$	Heat transfer capability of the stack	$J \cdot K^{-1} \cdot s^{-1}$
$U_{tank} A_{tank}$	Heat transfer capability of the tank	$J \cdot K^{-1} \cdot s^{-1}$
$U_{pipe} A_{pipe}$	Heat transfer capability of the pipe	$J \cdot K^{-1} \cdot s^{-1}$
$\Delta H_2$	Enthalpy change for reaction in vanadium specie $V^{2+}$	$J \cdot mol^{-1}$
$\Delta H_3$	Enthalpy change for reaction in vanadium specie $V^{3+}$	$J \cdot mol^{-1}$
$\Delta H_4$	Enthalpy change for reaction in vanadium specie $V^{4+}$	$J \cdot mol^{-1}$
$\Delta H_5$	Enthalpy change for reaction in vanadium specie $V^{5+}$	$J \cdot mol^{-1}$
$r$	Ohmic resistance of the stack	$\Omega$
$W_{pump}$	Pump power	W

### 475 5.3. Hydraulic model

476 A part of the system that has great importance is the hydraulic part. The pumps are dynamic  
 477 elements, and their choice in terms of the maximum flow rate they can pump, will depend on the  
 478 operating conditions of the system. For that reason, it is necessary to determine the power of the pump  
 479 need to make the electrolytes flow taking into account possible losses due to pressure and friction. The  
 480 power of the pump affects the temperature model, as can be seen from equation (23). Moreover, taking  
 481 into account that to maximize the efficiency of the VRFB, it is necessary to minimize losses (such as  
 482 pump power), the obtaining of a correct model will allow to obtain the optimal flow rate that plays the  
 483 most important role in a flow battery.

The value of the pump power can be obtained through the calculation of the losses in the stack and pipes, following the principle of energy conservation [126,127]. The power loss is the product between the pressure drop in the system and the flow rate  $Q$ :

$$W_{pump} = \Delta p \cdot Q. \quad (24)$$

484 The pressure drop in the pipes can be calculated using the principles of fluid mechanics. In some  
 485 studies, appears that it can be directly calculated considering two different parts. On the one hand, the  
 486 friction pressure drop  $\Delta p_{friction}$  which comes from fluid viscosity, which is calculated by (25) [127]. On  
 487 the other hand, the losses due to a change in flow direction of the pipes  $\Delta p_{pipes}$  given by equation (26).

$$\Delta p_{friction} = f \frac{L}{D_h} \frac{\rho v^2}{2}. \quad (25)$$

$$\Delta p_{pipes} = K \frac{\rho v^2}{2}. \quad (26)$$

488 The pressure drop in the stack can be calculated considering the pressure drop in the electrodes,  
 489 that have been found to contribute considerably to the total pressure drop of the system.

$$\Delta p_{el} = \frac{\mu \cdot Q \cdot K_{ck} \cdot (1 - \epsilon)^2}{d_f^2 \cdot \epsilon^3} \frac{L_{el}}{w_{el} \cdot t_{el}}. \quad (27)$$

Then, the pressure drop of the system is the sum of the previous pressure drops:

$$W_{pump} = (\Delta p_{friction} + \Delta p_{pipes} + \Delta p_{el}) \cdot Q. \quad (28)$$

490 Parameters of the hydraulic model are summarized in Table 9.

**Table 9.** Parameters of the hydraulic model.

Parameter	Meaning	Unit
$W_{pump}$	Pump power	W
$\epsilon$	Electrode porosity	-
$\mu$	Viscosity of the flow	$Pa \cdot s$
$f$	friction loss factor	-
$L$	Length of the pipe	m
$L_{el}$	Length of the electrodes	m
$D_h$	Hydraulic diameter of the pipe	$m^2$
$d_f$	mean diameter of the electrode fibers	m
$v$	Velocity of the flow rate	$m \cdot s^{-1}$
$K$	pipe loss factor due to the form	-
$K_{ck}$	Kozeny-Carman constant	-
$t_{el}$	Electrodes thickness	m
$w_{el}$	Electrodes width	m

#### 491 5.4. Summary of mathematical models

**Table 10.** RFB mathematical models classification.

	Lumped	Distributed
<b>Electrochemical</b>	[113] [114] [115] [119] [120] [121]	[107]
<b>Thermal</b>	[120] [121] [122] [123] [124] [125]	
<b>Hydraulic</b>	[126] [127]	[106] [108] [109]
<b>Equivalent circuit</b>	[116] [117] [118]	

## 492 6. Control and supervision

493 In this section, the main techniques which are currently used to control and automate RFB are  
 494 going to be described. The variables that are usually measured and used to regulate the RFB are the  
 495 current and the flow rate. The output variables of a RFB, typically are the stack voltage which is  
 496 directly related with the power, and the state of charge (SOC) of the system, which is related with the  
 497 stored or delivered energy.

### 498 6.1. Control strategy for RFB systems

499 For a RFB system, the control strategy plays a crucial role to guarantee the correct and optimal  
 500 operation of the battery for charge and discharge cycles, having a direct effect on the system efficiency.

501 The main variables to design a controller for RFB systems are the current, the stack voltage, the  
 502 temperature and the SOC. As mentioned, both the stack voltage and the current are easy variables  
 503 to measure, as well as the temperature. However, the SOC can not be measured so easily. For that  
 504 reason, there are different techniques to estimate its value, as will be seen later in section 6.2. Taking  
 505 into account these variables, there are different control strategies in the field of RFB that have been  
 506 implemented.

507 The most relevant objective in a RFB consists of guaranteeing that the system can store or provide  
 508 the required reactants during the charging/discharging process in a sure and efficient manner. Usually,  
 509 as the charged/discharged current is assumed to be externally fixed, the only variable that regulates  
 510 the operation of the battery is the flow rate. Therefore, the vast majority of control strategies are based  
 511 on obtaining the optimal flow according to the operational conditions. It is obvious that taking into  
 512 account that the operational conditions of the system vary, since it is dynamic, the optimal flow rate  
 513 will also be variant [128]. Therefore, these type of systems require to have pumps capable of providing  
 514 a variable flow in the system. The presence of pumps increases the losses inside the system due to the  
 515 energy consumption required to make them work. Moreover, the presence of hydraulic losses as the  
 516 ones presented in section 5.3, makes necessary to find a compromise between efficiency and safety

517 (understood as the possibility of guaranteeing reactants at all times and places). There exist different  
 518 strategies that are based on a mathematical expression, that define an optimal flow rate.

One of the most commonly used is based on the minimum flow. It appears in many studies, such as [11][129], and it is based on the Faraday's law of electrolysis:

$$Q_{min} = \begin{cases} \frac{N \cdot I}{F \cdot (1 - SOC) \cdot c_v}, & \text{for charging} \\ \frac{N \cdot |I|}{F \cdot SOC \cdot c_v}, & \text{for discharging} \end{cases} \quad (29)$$

where  $N$  is the number of cells that compose the stack, and  $c_v$  is the total concentration of vanadium in the solution. It expresses the theoretical minimum flow rate value of the RFB with respect to the current and the SOC, to guarantee that there are enough reactants in the system. Ideally, using that expression would be enough, but in practice due to its distributed nature using this value would not guarantee that there are enough reactants everywhere, or any desynchronization between the current and the controller would cause problems. Due to this, in most cases bigger values are used, by means of a constant called flow factor,  $FF$ , which typically varies between 4 to 10 [130].

$$Q = FF \cdot Q_{min} \quad (30)$$

519 The behaviour that presents this minimum flow rate with respect to the SOC and the current, has  
 520 been studied for the example of the RFB designed in section 3.3. Figure 4 shows the minimum flow for  
 521 both charging and discharging processes. A  $FF$  of 8 and a current range from 0 to 150 A have been  
 522 chosen. As can be noticed, using this strategy the flow rate must increase when the battery is near to  
 523 its full charge or discharge.

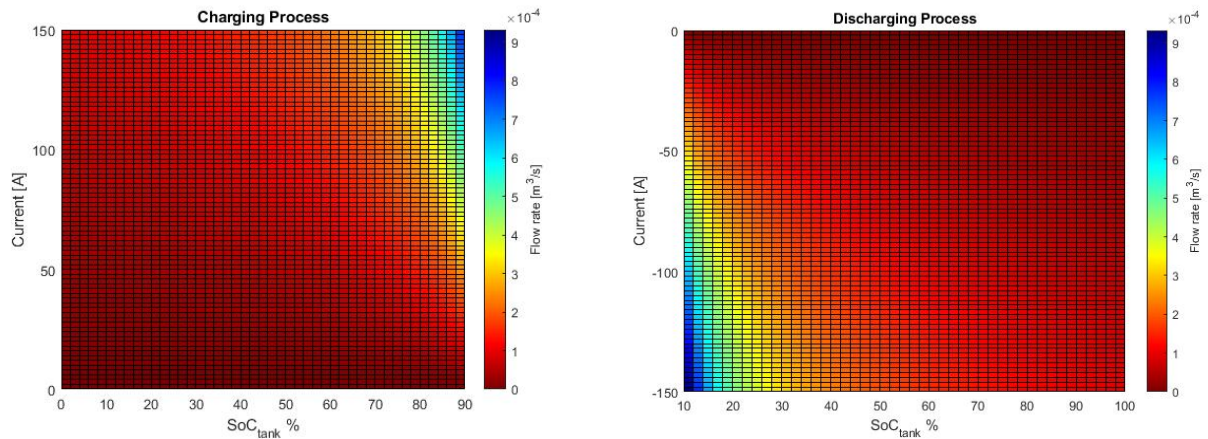


Figure 4. Minimum flow rate profiles for charging (left) and discharging (right) processes.

524 Other strategies are based on using an optimal flow rate that maximizes the efficiency of the  
 525 complete system taking into account the effect of the possible losses. The criterion to maximize the  
 526 battery efficiency is minimizing the system energy during the charging process and maximizing it  
 527 during discharge as is expressed in (31), within the same time window.

$$\mathcal{E}_{battery} = \begin{cases} \mathcal{E}_{stack} - \mathcal{E}_{pump} = \int P_{stack} dt - \int P_{pump} dt, & \text{during discharge} \\ \mathcal{E}_{stack} + \mathcal{E}_{pump} = \int P_{stack} dt + \int P_{pump} dt, & \text{during charge} \end{cases} \quad (31)$$

528

529

530 where  $\mathcal{E}_{stack}$  is the energy in the stack that can be affected by internal losses such as overpotentials,  
 531 and  $\mathcal{E}_{pump}$  is the power along the time from the pumps, taking into account the hydraulic losses.

532 There are different studies that use this criterion to develop an optimal flow rate strategy. [131]  
 533 presents a dynamic flow rate strategy for VRFB that takes into account the concentration overpotential  
 534 and the pump power consumption. In this area, Skyllas-Kazacos has also developed an optimal flow  
 535 rate strategy to maximize the efficiency of the battery at different charge and discharge processes [129].  
 536 Other studies such as [130,132,133] present optimal flow rate strategies to maximize the efficiency of  
 537 the battery system, minimizing the pump losses at the same time that maximize the power taking into  
 538 account the losses affected by the overpotential effect.

539 These optimal controllers are usually very sensitivity to uncertainty in the model and its  
 540 parameters; due to this, they are usually combined with other types of controllers. These new  
 541 strategies are based on regulating some variables, which typically is the stack voltage, using a feedback  
 542 controller and combine it with the optimal controller, which acts as a feedforward control law [134].  
 543 Another study uses a feedback controller to regulate the stack temperature [135] using a thermal model  
 544 based on [120], applying a variable flow rate to keep the temperature within safe limits, increasing the  
 545 efficiency of the system.

546 A general regulation scheme that considers an optimal flow rate strategy in terms of current and  
 547 SOC, and the regulation of the voltage corresponds to the architecture shown in Figure 5.

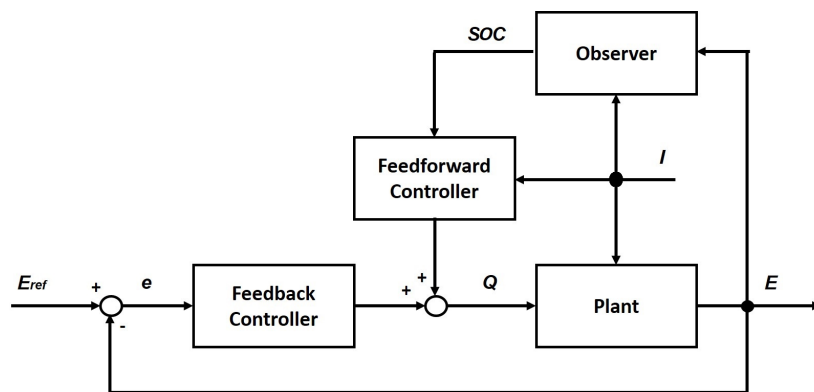


Figure 5. Conventional controller block scheme in a RFB.

548 Figure 5 presents a conventional controller scheme composed by a feedback controller that  
 549 regulates the voltage,  $E$ , and a feedforward controller. The current,  $I$ , is assumed to be an measurable  
 550 exogenous signal, and the SOC is obtained through an observer (section 6.2).

### 551 6.2. Observers and parameter estimation

552 SOC is one of the most important variables in RFB because it indicates how much energy is  
 553 stored in the system. Moreover, it is used in most control strategies, as shown in the previous section,  
 554 so obtaining its value is crucial for the proper functioning of these controllers. As it is shown in  
 555 (19), its value depends only in the concentration of vanadium species inside the electrolyte tanks.  
 556 Unfortunately, there is no sensor which allows to automatically measure this magnitude. There exist  
 557 different indirect techniques which allow to estimate the concentration of vanadium species inside  
 558 the tanks, i.e. estimate the SOC. One technique is the color analysis [136], based on the fact that  
 559 each vanadium species has its own color. Measuring the color inside the tank allows to estimate  
 560 the amount of vanadium species, and therefore, the SOC. Another technique to estimate the SOC is  
 561 measuring the electrolyte density inside the tanks [137]. Similarly, to what happens with color, each  
 562 vanadium species has its own density. Spectrophotometric can be used to analyze the conductivity of  
 563 the vanadium species contained in the tank, this technique is widely used in chemical studies to obtain  
 564 the concentration of certain species dissolved in a solution [138]. Recently, the use of an amperimetric  
 565 sensor [139] has been proposed. It estimates the vanadium species by measuring the current response  
 566 at a fixed stack voltage.

567 All these techniques require incorporating sophisticated and expensive instrumentation into  
 568 the system. This increases the cost of the installation in addition to its complexity. Most of these  
 569 techniques are indirect measurements and therefore require significant calibration and sophisticated  
 570 post-processing. An additional problem that must be taken into account is that the storage tanks are  
 571 normally large, which implies that the distribution of the species is not homogeneous and therefore  
 572 low precision exists despite having sophisticated instrumentation.

573 An alternative way of dealing with the problem is to use the model and easily measurable  
 574 information, such as stack voltage, current or temperature, to estimate the variables of interest. The use  
 575 of state observers and parameter estimators can be a very efficient solution to estimate the SOC. Apart  
 576 from the SOC, there are other highly relevant variables, that must be estimated since their theoretical  
 577 values differ from those found in practice and can not be directly measured. Different methodologies  
 578 are discussed in the following subsections.

### 579 6.2.1. State observers to estimate the SOC

580 State observers are algorithms that allow estimating the value of state variables, whose evolution  
 581 is described by the system model, combining the use of the model and information from the measured  
 582 variables [140,141]. In Figure 6 it is shown an scheme of a state observer with its main blocks and  
 583 variables, where  $\hat{x}$  corresponds to the state estimation,  $u$  is the input control action,  $y$  is the output  
 584 measured,  $p$  corresponds to the model parameters,  $f$  represents the model,  $h$  is the output computation  
 585 function,  $\Phi$  is the correction action function and  $v$  is the correction control action.

586 There are different techniques to design these algorithms, being Kalman filters and sliding mode  
 587 observers two of the most popular [142].

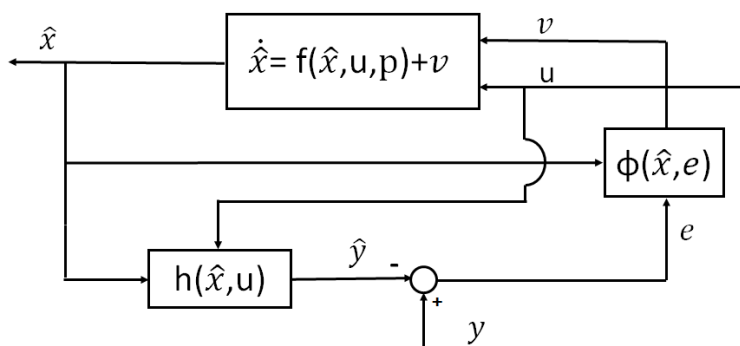


Figure 6. State observer scheme.

588 In the models described in the section 5, tank concentrations are state variables, from which the  
 589 SOC can easily be estimated using (19). Therefore, it is possible to build state observers that allow  
 590 estimating the SOC in real-time. Table 11 summarizes the states observers found in the literature, with  
 591 their measured variables and methods used to estimate the SOC.

592 Based on conductivity and spectrophotometric measurements, Skyllas-Kazacos presented two  
 593 estimation methods for the SOC in [138]. The first method uses variations in conductivity to  
 594 independently determine the SOC of each half-cell electrolyte. The second approach is based on  
 595 the optical absorbance detected to monitor the system balance and SOC of the negative half-cell.

596 Using the measures of half-cell potential and electrolyte density, and an electrochemical model  
 597 it has also been also possible to estimate the SOC as it is presented in [137]. This study presents two  
 598 approaches. The first one, measures the OCV combined with Coulomb counting, to estimate the SOC  
 599 assuming the same concentrations of vanadium species inside the tanks and the cell. The second  
 600 approach, uses the temperature and electrolyte density measurements for estimate the SOC. Both  
 601 strategies can be recalibrated during the battery operation increasing the reliability of the estimation.



602 The thermal model described in section 5.2, is used in [143], with a Kalman filter to estimate SOC  
 603 precisely. An electrical model is defined using the cell voltage which varies with the stack temperature,  
 604 and the cell concentrations. In this way, measuring both cell voltage and temperature is possible to  
 605 obtain the SOC estimation. Another electrical model is proposed in [144], which consists on a basic  
 606 resistor-capacitor (RC) ladder. The capacity of a RFB represents the amount of energy that can be  
 607 extracted under certain specified conditions [145]. Therefore, it has a direct dependence on the stored  
 608 energy, and thus, on the SOC. Measuring the cell voltage and with the aim of a Kalman filter the SOC  
 609 is estimated.

610 The extended Kalman filter (EKF) is one of the widely methods used to estimate the SOC of RFB  
 611 systems [146–148]. In those cases, electrochemical and thermal models, as well as OCV expression  
 612 are used to estimate the SOC. Adaptive estimation techniques have also been used to estimated with  
 613 precision the SOC, using similar models. [149] presents an adaptive observer design for simultaneous  
 614 estimation of SOC and crossover flux, for a nonaqueous RFB that is simply modelled with a isothermal  
 615 lumped parameter model, measuring the temperature and the flow rate. Another adaptive technique  
 616 is proposed in [150], which consists on a novel joint real time estimator based on the EKF, which  
 617 estimates the SOC using the recursive least squares (RLS) method, measuring the OCV and the current.

618 Differently from the Kalman and the EKF which requires linearizing the model, sliding mode  
 619 control (SMC) can directly deal with nonlinear models. This is the case of [151,152], that use sliding  
 620 mode observers to predict the value of the SOC. For both cases, the model used is based on the  
 621 conservation of mass and energy, as the ones shown in the electrochemical and thermal model part, in  
 622 section 5.1 and section 5.2, respectively.

623 An empirical neural network (NN) is employed in [153] to estimate the SOC measuring the  
 624 temperature and the viscosity of the electrolyte. In that case, by means of Nerst equation, an empirical  
 625 model is develop that links the SOC with respect to the temperature and viscosity of the electrolyte.

626 Other intelligent methods such as fuzzy logic (FL) [154] or support vector machines (SVM)  
 627 [155,156] have been also used to estimate the SOC. They perform the estimation by analyzing the data  
 628 provided from different experiments on wide operational ranges. [154] involves the fuzzy logic to  
 629 analyze impedance spectroscopy and coulomb counting measures. In terms of SVM, [155] uses data  
 630 to estimate the SOC and model parameters from charging/discharging data, using the current, the  
 631 voltage and the temperature of a cell. [156] uses both current and temperature to estimate the SOC  
 632 using a thermal dependant model.

**Table 11.** Summary of SOC observers with their measurement variables (KF: Kalman filter; EKF: Extended Kalman filter; SMC: Slisind mode control; NN: Neural network; SVM: Support vector machines; FL: Fuzzy logic).

	KF/EKF	SMC	NN	SVM	FL
<b>Voltage/Current</b>	[144] [150] [137]	[151] [152]		[155] [156]	[154]
<b>Flow rate</b>	[149]				
<b>Temperature</b>	[143] [149] [137]	[151] [152]	[153]	[155] [156]	
<b>Density</b>	[137]		[153]		
<b>Conductivity</b>	[138]				[154]

### 633 6.2.2. Model tuning and parameter estimation

634 The models described, including those used in observer development, contain a large number  
 635 of parameters that must be adjusted. Although many of these parameters could be measured, it is a  
 636 current trend to adjust the models using the variables usually measured.

637 These adjustments can be made following two types of approaches, depending on whether  
 638 the estimation is done in real time or not. **Online parameter estimation** is based on updating the  
 639 estimation when new information is available. Thus, the estimation is make in real-time [30]. This  
 640 adjustment only needs a parameter estimation algorithm that calibrates the model parameters each time  
 641 it receives information for the input signals and measured variables. **Offline parameter estimation** is

642 made with data that has been previously acquired [157]. Firstly, it estimates the output variables that  
 643 can not measure in real time, to compare with real data that has been previously acquired. Then, takes  
 644 place the tuning of parameters minimizing the error between the variables estimated and the real ones.  
 645 Figure 7 shows the schemes of each one of these approaches.

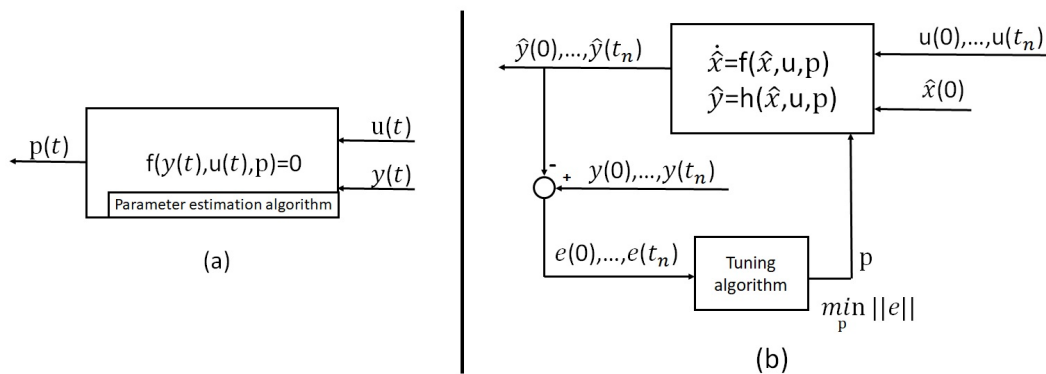


**Figure 7.** Parameter estimation schemes. (a) Online parameter estimation, (b) Offline parameter estimation.

646 Examples of this type of parameters that present uncertainty are the diffusion coefficients,  $k$ ,  
 647 appearing in (15), the standard electrode potential,  $E^0$ , (2) or the charge/discharge resistance  $r$ . Usually,  
 648 all these values are assumed to be constant to facilitate the analysis of the model carried out. In [158]  
 649 an offline estimation of stack resistance and standard electrode potential is presented, using the least  
 650 square method for the curve fitting between the experimental data and the model, measuring the  
 651 current and the stack voltage of the battery.

652 Other type of variables appearing in RFB models are the capacity loss or the peak power, which  
 653 consists on the maximum point of power that the VRFB can supply taking into account the operational  
 654 conditions in terms of current and voltage. Capacity fading appears when VRFB work long and causes  
 655 the ion diffusion and depletion of active materials. This yields not only to a capacity loss, but also  
 656 to an increasing of the internal resistance [152]. There are several studies that estimate the capacity  
 657 fading using online estimation methods, being one of the most common techniques the EKF. [150]  
 658 uses this technique to online estimate the capacity loss, and the parameters of an electrical model,  
 659 measuring the OCV and the current. A similar approach is presented in [159], measuring the same  
 660 variables, and using a first-order electrical circuit model to capture the dynamics of the VRFB. Using  
 661 the RLS method with the EKF technique, the model parameters and the capacity are online estimated  
 662 with high accuracy. [160] differs from the previous two studies using an autoregressive exogenous  
 663 model to estimate the capacity loss, measuring with an H-infinity observer the current, the voltage  
 664 and the temperature of the stack.

665 In terms of peak power, [161] uses an adaptive model that allows to estimate its value. Using  
 666 the RLS and the EKF an online adaptive estimation of the RFB parameters is obtained and by means of  
 667 measuring the current and voltage of the system.

668 [162,163] propose an algorithm to online estimate different parameters using a time-varying  
 669 recursive least squares method. These parameters are the resistors and capacities of a second order  
 670 Thevenin model used to characterize a VRFB. Both studies use data from pulse charging experiments,  
 671 measuring the current and voltage.

672 Using genetic algorithm, it is also possible to offline estimate the different parameters of a RFB  
 673 model as is presented in [157], measuring the voltage. In that case, the parameters of the model define  
 674 the electrolyte properties, such as the diffusion and the transfer function coefficients, the electrode  
 675 and membrane properties, the electrode porosity or specific surface area. Finally, a multi-time scale  
 676 method is used in [164] to online estimate independently the model parameters and OCV, measuring  
 677 the current, temperature, flow rate and density.

## 678 7. Conclusions and future direction

679 This paper has introduced the concept of redox flow batteries, contextualizing them within the  
680 current energy situation and comparing them with other type of energy storage systems.

681 The main characteristics and its operation have been explained taking into account the equations  
682 that characterize its behaviour, as well as the expressions needed to design the battery sizing for a  
683 specific conditions of power and energy. A review in the literature of the existing models has been  
684 shown, explaining in detail one of the most used and cited. This dynamic model is decomposed in  
685 three main parts that are interconnected: the electrochemical, the thermal and the hydraulic. Attending  
686 to the need for optimal control and characterization of the RFB, a discussion about the existing control  
687 strategies that are mainly used within the field of redox flow batteries has been presented. Similarly, a  
688 discussion about the different methods used to estimate the SOC has been presented, introducing the  
689 use of state observers. Finally, some studies have been presented that calibrate the models estimating  
690 their parameters and variables. All these techniques constitute an excellent alternative to include  
691 complex and expensive instrumentation in the RFB. It has been prove in the literature that these  
692 techniques offer very interesting results.

693 Modelling plays a key role for control purposes inside the RFB. It allows to described the real  
694 system behaviour, providing information and knowledge of the system operation. Moreover, these  
695 models are very important to analyse and improve the control systems, observers and parameter  
696 estimators. In this sense, until now different studies have been designed with the purpose to obtain a  
697 realistic model of a VRFB. Most of them are lumped parameter models that describe with simplicity  
698 the behaviour of the RFB, obtaining a behavior which closely resembles the real system. There are few  
699 studies that present more complex models that take into account undesired effects such as corrosion,  
700 degradation or unexpected reactions. In this scenario, more research will appear in the following years  
701 to manage with more realistic models, that will allow to perform more tests to analyze the behaviour  
702 of a specific RFB, reducing the R&D (Research and Development) costs. For these purposes, it will  
703 be necessary to analyze in which scenarios the use of a lumped or distributed parameter model will  
704 be the best option, attending to the practical use that will be given to it. Furthermore, if a distributed  
705 parameter model is selected, an analysis of the level of distribution will be required.

706 Looking to the future, there are different directions in the research of RFB systems. Within the  
707 field of control and supervision, research in terms of flow management and parameter estimation  
708 will continue to grow, following methodologies such as those described in section 6. In particular,  
709 the search for online estimators will be one of the key studies in the future, to estimate the different  
710 parameters. Therefore, integrating these parameters in the control laws will improve their robustness.  
711 Inside this field, a determination of the main parameters to estimate will be required. In addition,  
712 parameters that vary over the time and are currently considered constant to simplify the analysis,  
713 such as the ohmic resistance or the standard electrode potential, will be online estimated obtaining a  
714 more realistic adjustment. It will also be necessary to determine what parameters are affected by the  
715 undesired effects such as degradation or corrosion, and its level of affection. As a battery system, it  
716 will be important to define the state of health (SOH) which until now has not been studied in detail.  
717 Another field of study will be the detection of failures, characterizing the possible failures, what they  
718 are due to and the level of damage that they cause within the system. Taking into account all these  
719 objectives, a large number of experimental tests will be carried out, being decisive to correctly define  
720 the working conditions, the variables to be measured and the instrumentation to be used, seeking a  
721 balance between efficiency and experimental cost.

722 The automation will contribute to the reduction of costs and will open the door to the  
723 implementation of fault detection and isolation mechanisms. This will improve their performance and  
724 make them even more secure and reliable devices.

725 Other important investigations will correspond to develop an efficient integration of RFB's in  
726 energetic environments such as renewable energy plants, or microgrids.

727 **Author Contributions:** Conceptualization, R.C. and A.C.; methodology, R.C. and A.C.; investigation, R.C. and  
 728 A.C.; writing—original draft preparation, A.C.; writing—review and editing, R.C.; visualization, A.C.; supervision,  
 729 R.C.; project administration, R.C.; funding acquisition, R.C. All authors have read and agreed to the published  
 730 version of the manuscript.

731 **Funding:** This research was funded by the CSIC under the PTI FLOWBAT 2021 project (reference: 642 201980E101),  
 732 the Spanish Ministry of Economy and Competitiveness under Projects CICYT RTI2018-094665-B-I00, DOVELAR ref.  
 733 RTI2018-096001-B-C32 (MCIU/AEI/FEDER, UE) and María de Maeztu Seal of Excellence to IRI (MDM-2016-0656),  
 734 and by the *Generalitat de Catalunya* through the Project 2017 SGR 482.

735 **Conflicts of Interest:** The authors declare no conflict of interest.

## 736 Abbreviations

737 The following abbreviations are used in this manuscript:

738 CAES	Compressed air energy storage
CEM	Cation exchange membrane
EDLC	Electric double layer capacitor
ESS	Energy storage systems
EKF	Extended Kalman filter
FL	Fuzzy logic
NN	Neural network
OCV	Open circuit voltage
PHES	Pumped hydro energy storage
739 RES	Renewable energy sources
RFB	Redox flow battery
RFC	Regenerative fuel cell
SMC	Sliding mode control
SMES	Superconducting magnetic energy storage
SOC	State of charge
SOH	State of health
SVM	Support vector machines
UPS	Uninterruptible power supply
VRFB	Vanadium redox flow battery

## 740 References

- 741 1. Martins, F.; Felgueiras, C.; Smitkova, M.; Caetano, N. Analysis of Fossil Fuel Energy Consumption and  
 742 Environmental Impacts in European Countries. *Energies* **2019**, *12*. doi:10.3390/en12060964.
- 743 2. Van den Bergh, J.; Botzen, W. Monetary valuation of the social cost of CO<sub>2</sub> emissions: A critical survey.  
 744 *Eco. Eco.* **2015**, *114*, 33–46. doi:https://doi.org/10.1016/j.ecolecon.2015.03.015.
- 745 3. Üney, M.; Çetinkaya, N. Comparison of CO<sub>2</sub> emissions fossil fuel based energy generation plants and  
 746 plants with Renewable Energy Source. *6th Int. Conf. Elec. Com. Art. Int.* **2014**, *20*, 29–34.
- 747 4. Caetano, N.S.; Mata, T.M.; Martins, A.A.; Felgueiras, M.C. New Trends in Energy Production and  
 748 Utilization. *Energy Pro.* **2017**, *107*, 7–14. doi:https://doi.org/10.1016/j.egypro.2016.12.12.
- 749 5. Gielen, D.; Boshell, F.; Saygin, D.; Bazilian, M.D.; Wagner, N.; Gorini, R. The role of renewable energy in the  
 750 global energy transformation. *En. Str. Rev.* **2019**, *24*, 38–50. doi:https://doi.org/10.1016/j.esr.2019.01.006.
- 751 6. Peker, M.; Kocaman, A.S.; Kara, B.Y. Benefits of transmission switching and energy storage in  
 752 power systems with high renewable energy penetration. *Applied. Energies.* **2018**, *228*, 1182–1197.  
 753 doi:https://doi.org/10.1016/j.apenergy.2018.07.008.
- 754 7. Root, C.; Presume, H.; Proudfoot, D.; Willis, L.; Masiello, R. Using battery energy storage to reduce  
 755 renewable resource curtailment. *IEEE Pow. En. ISGTC* **2017**, *1*, 1–5. doi:10.1109/ISGT.2017.8085955.
- 756 8. Padiyar, K.R.; Kulkarni, A.M. Solar Power Generation and Energy Storage. *Dyn. and Control of El. Trans.*  
 757 *and Microgrids* **2019**, pp. 391–414. doi:10.1002/9781119173410.ch11.
- 758 9. Lu, M.; Chang, C.; Lee, W.; Wang, L. Combining the Wind Power Generation System With Energy Storage  
 759 Equipment. *IEEE Trans. Ind. App.* **2009**, *45*, 2109–2115. doi:10.1109/TIA.2009.2031937.

- 760 10. Das, C.K.; Bass, O.; Kothapalli, G.; Mahmoud, T.S.; Habibi, D. Overview of energy storage systems in  
761 distribution networks: Placement, sizing, operation, and power quality. *Ren. Sust. Energy* **2018**, *91*, 1205–  
762 1230. doi:<https://doi.org/10.1016/j.rser.2018.03.068>.
- 763 11. Blanc, C. Modeling of a Vanadium Redox Flow Battery Electricity Storage System **2009**.  
764 doi:10.5075/epfl-thesis-4277.
- 765 12. Mallick, K.; Das, S.; Sengupta, A.; Chattaraj, S. Modern Mechanical Energy Storage  
766 Systems and Technologies. *Int. Journal Eng. Res. Tech. (IJERT)* **2016**, *5*, 727–730.  
767 doi:<http://dx.doi.org/10.17577/IJERTV5IS020649>.
- 768 13. Yang, C.J.; Jackson, R. Opportunities and barriers to pumped-hydro energy storage in the united states.  
769 *Ren. Sust. Energy Reviews* **2011**, *15*, 839–844. doi:<https://doi.org/10.1016/j.rser.2010.09.020>.
- 770 14. Hernández, J.; Gyuk, I.; Christensen, C. DOE global energy storage database — A platform for large scale  
771 data analytics and system performance metrics. *2016 IEEE Int. Conf. Power System Tech. (POWERCON)*  
772 **2016**, *1*, 1–6. doi:10.1109/POWERCON.2016.7754009.
- 773 15. Chen, R.; Kim, S.; Chang, Z., Large-scale energy storage. In *Redox Flow Batteries: Fundamentals and*  
774 *Applications*; Zhanga, H.; Li, X.; Zhang, J., Eds.; CRC Press, 2018; pp. 3–43. doi:10.5772/intechopen.68752.
- 775 16. Chen, L.; Zheng, T.; Mei, S.; Xue, X.; Liu, B.; Lu, Q. Review and prospect of compressed  
776 air energy storage system. *Journal of Modern Power Systems and Clean Energy* **2016**, *4*, 529–541.  
777 doi:<https://doi.org/10.1007/s40565-016-0240-5>.
- 778 17. Succar, S.S.; Williams, R.H.; Cavallo, A.J.; Christopher, C.K.; Nrel, P.D.; Denkenberger, D.; Kalinowski,  
779 A.; McGill, M.; Socolow, R.H.; Vann, I.R. Compressed Air Energy Storage : Theory , Resources , And  
780 Applications For Wind Power. *Princ. Env. Ins. Rep., Princeton University* **2008**, *37*, 3149–3158.
- 781 18. Crotofino, F.; Mohmeyer, K.U.; Scharf, R. Huntorf CAES: More than 20 Years of Successful Operation. *Nat*  
782 *Gas* **2001**, *45*.
- 783 19. Mukherjee, P.; Rao, V. Superconducting magnetic energy storage for stabilizing grid integrated  
784 with wind power generation systems. *Modern Power Systems and Clean Energy* **2019**, *7*, 400–411.  
785 doi:<https://doi.org/10.1007/s40565-018-0460-y>.
- 786 20. Chen, L.; Liu, Y.; Arsoy, A.; Ribeiro, P.; Steurer, M.; Iravani, M. Detailed modeling of  
787 superconducting magnetic energy storage (SMES) system. *IEEE Tr. Pow. Del.* **2006**, *21*, 699–710.  
788 doi:<https://doi.org/10.1109/TPWRD.2005.864075>.
- 789 21. Wagner, L., Overview of Energy Storage Technologies. In *Future Energy*, Second edition ed.; Letcher, T.M.,  
790 Ed.; Elsevier: Boston, 2014; pp. 613–631. doi:<https://doi.org/10.1016/B978-0-08-099424-6.00027-2>.
- 791 22. Vangari, M.; Pryor, T.; Jiang, L. Supercapacitors: Review of materials and fabrication methods. *Energy Eng.*  
792 **2013**, *139*, 72–79. doi:[https://doi.org/10.1061/\(ASCE\)EY.1943-7897.0000102](https://doi.org/10.1061/(ASCE)EY.1943-7897.0000102).
- 793 23. Poullikkas, A. A comparative overview of large-scale battery systems for electricity storage. *Ren. and Sust.*  
794 *En. Rev.* **2013**, *27*, 778–788. doi:<https://doi.org/10.1016/j.rser.2013.07.017>.
- 795 24. Linden, D.; Reddy, T., Lead-Acid batteries. In *Handbook of batteries*; handbooks, M.H., Ed.; McGraw-Hill:  
796 New York, 2002; pp. 1–88.
- 797 25. Rydh, C. Environmental assessment of vanadium redox and lead-acid bat-teries for stationary energy  
798 storage. *Power Sources* **1999**, *1*, 21–29. doi:[https://doi.org/https://doi.org/10.1016/S0378-7753\(98\)00249-3](https://doi.org/https://doi.org/10.1016/S0378-7753(98)00249-3).
- 799 26. Wen, Z.; Cao, J.; Gu, Z.; Xu, X.; Zhang, F.; Lin, Z. Research on sodium sulfur battery for energy storage.  
800 *Solid State Ionics* **2008**, *179*, 1697–1701. doi:<https://doi.org/10.1016/j.ssi.2008.01.070>.
- 801 27. Oshima, T.; Kajita, M.; Okuno, A. Development of sodium-sulfur batteries. *Int. Journal of App. Cer. Tech.*  
802 **2005**, *1*, 269–276. doi:<https://doi.org/10.1111/j.1744-7402.2004.tb00179.x>.
- 803 28. Korthauer, R., Lithium-Ion Batteries. In *Lithium-Ion Batteries: Basics and Applications*; Korthauer, R., Ed.;  
804 Springer: New York, 2018. doi:10.1007/978-3-662-53071-9.
- 805 29. Li, J.; Murphy, E.; Winnick, J.; Kohl, P. Studies on the cycle life of commercial lithium ion  
806 batteries during rapid charge–discharge cycling. *Journal of Power Sources* **2001**, *102*, 294–301.  
807 doi:[https://doi.org/10.1016/S0378-7753\(01\)00821-7](https://doi.org/10.1016/S0378-7753(01)00821-7).
- 808 30. Xing, Y.; Na, J.; Costa-Castelló, R. Real-Time Adaptive Parameter Estimation for a Polymer  
809 Electrolyte Membrane Fuel Cell. *IEEE Transactions on Industrial Informatics* **2019**, *15*, 6048–6057.  
810 doi:10.1109/TII.2019.2915569.

- 811 31. Cecilia, A.; Costa Castelló, R. Observador de alta ganancia con zona muerta ajustable para estimar la  
812 saturación de agua líquida en pilas de combustible tipo PEM. *Revista Iberoamericana de Automática e*  
813 *Informática Industrial* **2020**, *2*, 169–180. doi:<https://doi.org/10.17979/spudc.9788497497169.382>.
- 814 32. Andrews, J.; Doddathimmaiah, A., Regenerative fuel cells. In *Materials for Fuel Cells*; Gasik, M., Ed.;  
815 Woodhead Publishing Series in Electronic and Optical Materials, Woodhead Publishing, 2008; pp. 344 –  
816 385. doi:<https://doi.org/10.1533/9781845694838.344>.
- 817 33. Wang, Y.; Leung, D.Y.; Xuan, J.; Wang, H. A review on unitized regenerative fuel cell technologies, part-A:  
818 Unitized regenerative proton exchange membrane fuel cells. *Renewable and Sustainable Energy Reviews* **2016**,  
819 *65*, 961 – 977. doi:<https://doi.org/10.1016/j.rser.2016.07.046>.
- 820 34. Hou, Y.; Zhuang, M.; Wan, G. The analysis for the efficiency proper-ties of the fuel cell engine. *Renewable*  
821 *Energy* **2007**, *32*, 1175–1186. doi:<https://doi.org/10.1016/j.renene.2006.04.012>.
- 822 35. Cecilia, A.; Carroquino, J.; V., R.; Costa Castelló, R.; Barreras, F. Optimal energy management in a standalone  
823 microgrid, with photovoltaic generation, short-term storage, and hydrogen production. *Energies* **2020**,  
824 *13*, 1454. doi:<https://doi.org/10.3390/en13061454>.
- 825 36. Salameh, Z., Energy storage. In *Renewable Energy System Design*; Salameh, Z., Ed.; Academic Press: Boston,  
826 2014. doi:<https://doi.org/10.1016/B978-0-12-374991-8.00004-0>.
- 827 37. Shigematsu, T. Redox flow battery for energy storage. *SEI Technical Review* **2011**, *73*, 4–13.
- 828 38. Alotto, P.; Guarneri, M.; Moro, F.; Stella, A. Redox Flow Batteries for large scale energy storage **2012**.  
829 *1*, 293–298. doi:10.1109/EnergyCon.2012.6347770.
- 830 39. Noack, J.; Wietschel, L.; Roznyatovskaya, N.; Pinkwart, K.; Tübke, J. Techno-Economic Modeling and  
831 Analysis of Redox Flow Battery Systems **2016**. *9*, 627. doi:<https://doi.org/10.3390/en9080627>.
- 832 40. Ye, R.; Henkensmeier, D.; Yoon, S.J.; Huang, Z.; Kim, D.K.; Chang, Z.; Kim, S.; Chen, R. Redox Flow  
833 Batteries for Energy Storage: A Technology Review. *Journal of Elec. En. Conv. and Sto.* **2017**, *15*, 010801.  
834 doi:10.1115/1.4037248.
- 835 41. Fujimoto, C.; Kim, S.; Stains, R.; Wei, X.; Li, L.; Yang, Z.G. Vanadium redox flow battery efficiency and  
836 durability studies of sulfonated Diels Alder poly(phenylene)s. *Electrochemistry Communications* **2012**, *20*, 48  
837 – 51. doi:<https://doi.org/10.1016/j.elecom.2012.03.037>.
- 838 42. Ibrahim, H.; Ilinca, A.; Perron, J. Energy storage systems—Characteristics and comparisons. *Renewable and*  
839 *Sustainable Energy Reviews* **2008**, *12*, 1221 – 1250. doi:<https://doi.org/10.1016/j.rser.2007.01.023>.
- 840 43. Uhrig, M.; Koenig, S.; Suriyah, M.R.; Leibfried, T. Lithium-based vs. Vanadium Redox Flow  
841 Batteries – A Comparison for Home Storage Systems. *Energy Procedia* **2016**, *99*, 35 – 43. 10th  
842 International Renewable Energy Storage Conference, IRES 2016, 15-17 March 2016, Düsseldorf, Germany,  
843 doi:<https://doi.org/10.1016/j.egypro.2016.10.095>.
- 844 44. Vermeer, W.; Chandra Mouli, G.R.; Bauer, P. Real-Time Building Smart Charging System Based on PV  
845 Forecast and Li-Ion Battery Degradation. *Energies* **2020**, *13*. doi:10.3390/en13133415.
- 846 45. Or, T.; Gourley, W.; Kaliyappan, K.; Yu, A.; Chen, Z. Recycling of mixed cathode lithium-ion  
847 batteries for electric vehicles: Current status and future outlook. *Carbon energy* **2020**, *2*, 6–43.  
848 doi:<https://doi.org/10.1002/cey2.29>.
- 849 46. Xiao, B.; Xiao, B.; Liu, L. State of Health Estimation for Lithium-Ion Batteries Based  
850 on the Constant Current–Constant Voltage Charging Curve. *Electronics* **2020**, *9*, 1279.  
851 doi:<https://doi.org/10.3390/electronics9081279>.
- 852 47. Vermeer, W.; Chandra Mouli, G.; Bauer, P. Real-Time Building Smart Charging System Based on PV  
853 Forecast and Li-Ion Battery Degradation. *Energies* **2020**, *13*, 3415. doi:<https://doi.org/10.3390/en13133415>.
- 854 48. Bian, X.; Liu, L.; Yan, J.; Zou, Z.; Zhao, R. An open circuit voltage-based model for state-of-health estimation  
855 of lithium-ion batteries: Model development and validation. *Journal of Power Sources* **2020**, *448*, 227401.  
856 doi:<https://doi.org/10.1016/j.jpowsour.2019.227401>.
- 857 49. Gatti, D., Redox Flow Batteries’ Advantages for Stationary Energy Storage Market; 2020 (accessed May 11,  
858 2020).
- 859 50. Noack, J. *Fraunhofer ICT - Redox Flow Battery Group*, 2016 (accessed May 11, 2020).  
860 doi:10.13140/RG.2.1.1440.9207.
- 861 51. Jiang, H.; Sun, J.; Wei, L.; Wu, M.; Shyy, W.; Zhao, T. A high power density and  
862 long cycle life vanadium redox flow battery. *Energy Storage Materials* **2020**, *24*, 529 – 540.  
863 doi:<https://doi.org/10.1016/j.ensm.2019.07.005>.



- 864 52. Zhang, C.; Zhao, T.; Xu, Q.; An, L.; Zhao, G. Effects of operating temperature on  
865 the performance of vanadium redox flow batteries. *Applied Energy* **2015**, *155*, 349 – 353.  
866 doi:<https://doi.org/10.1016/j.apenergy.2015.06.002>.
- 867 53. Jizhong, C.; Hou, C.; Wu, G.; Wang, K.; Mao, H.; Dong, H. Research on Self-discharge Characteristics  
868 of a Vanadium Redox-flow Battery System. *DEStech Tran. on Env., Energy and Earth Science* **2016**.  
869 doi:10.12783/dteees/peee2016/3835.
- 870 54. Zhang, D.; Liu, Q.; Li, Y. Chapter 3 - Design of flow battery **2014**. pp. 61 – 97.  
871 doi:<https://doi.org/10.1016/B978-0-444-59566-9.00003-X>.
- 872 55. Zeng, Y.; Zhou, X.; An, L.; Wei, L.; Zhao, T. A high-performance flow-field structured  
873 iron-chromium redox flow battery. *Journal of Power Sources* **2016**, *324*, 738 – 744.  
874 doi:<https://doi.org/10.1016/j.jpowsour.2016.05.138>.
- 875 56. Suresh, S.; Kesavan, T.; Yeddala, M.; Arulraj, I.; Dheenadayalan, S.; Ragupathy, P. Zinc-bromine  
876 hybrid flow battery: Effect of zinc utilization and performance characteristics. *RSC Adv.* **2014**, *4*.  
877 doi:10.1039/C4RA05946H.
- 878 57. Cunha, J.; Martins, J.; Rodrigues, N.; Brito, F. Vanadium redox flow batteries: A technology review. *Int.*  
879 *Journal of En. Res.* **2014**, *39*, 889–918. doi:10.1002/er.3260.
- 880 58. Chen, R.; Kim, S.; Chang, Z. Redox Flow Batteries: Fundamentals and Applications [open access] **2017**. pp.  
881 103–118. doi:10.5772/intechopen.68752.
- 882 59. Yuan, X.; Song, C.; Platt, A.; Zhao, N.; Wang, H.; Li, H.; Fatih, K.; Jang, D. A review of all-vanadium redox  
883 flow battery durability: Degradation mechanisms and mitigation strategies. *International Journal of Energy*  
884 *Research* **2019**, *43*. doi:10.1002/er.4607.
- 885 60. Chen, H.; Cong, G.; Lu, Y.C. Recent progress in organic redox flow batteries: Active  
886 materials, electrolytes and membranes. *Journal of Energy Chemistry* **2018**, *27*, 1304 – 1325.  
887 doi:<https://doi.org/10.1016/j.jechem.2018.02.009>.
- 888 61. Alotto, P.; Guarnieri, M.; Moro, F. Redox flow batteries for the storage of renewable energy: A review. *Ren.*  
889 *Sust. Energy Review* **2014**, *29*, 325–335. doi:<https://doi.org/10.1016/j.rser.2013.08.001>.
- 890 62. Clark, J. *Definitions of oxidation and reduction (REDOX)*, 2003 (accessed May 5, 2020).  
891 doi:<https://www.chemguide.co.uk/inorganic/redox/definitions.html>.
- 892 63. Kim, K.; Park, M.S.; Kim, Y.; Kim, J.H.; Dou, S.; Skyllas-Kazacos, M. A technology review of electrodes and  
893 reaction mechanisms in vanadium redox flow batteries. *Journal of Materials Chemistry* **2015**, *3*, 16913–16933.  
894 doi:10.1039/C5TA02613J.
- 895 64. Fan, X.; Liu, J.; Yan, C., "Chapter 4: Key Materials of Vanadium Flow Batteries: Electrodes" in "Redox Flow  
896 Batteries: Fundamentals and Applications"; 2017; pp. 127–217.
- 897 65. Ke, X.; Prah, J.M.; Alexander, J.I.D.; Savinell, R.F. Rechargeable redox flow batteries: Maximum current  
898 density with electrolyte flow reactant penetration in a serpentine flow structure, 2017.
- 899 66. Ke, X.; Prah, J.M.; Alexander, J.I.D.; Wainright, J.S.; Zawodzinski, T.A.; Savinell, R.F. Rechargeable  
900 redox flow batteries: flow fields, stacks and design considerations. *Chem. Soc. Rev.* **2018**, *47*, 8721–8743.  
901 doi:10.1039/C8CS00072G.
- 902 67. Melke, J.; Jakes, P.; Langner, J.; Riekehr, L.; Kunz, U.; Zhao-Karger, Z.; Nefedov, A.; Sezen, H.; Wöll, C.;  
903 Ehrenberg, H.; Roth, C. Carbon materials for the positive electrode in all-vanadium redox flow batteries.  
904 *Carbon* **2014**, *78*, 220 – 230. doi:<https://doi.org/10.1016/j.carbon.2014.06.075>.
- 905 68. Chen, J.Y.; Hsieh, C.L.; Hsu, N.Y.; Chou, Y.S.; Chen, Y.S. Determining the Limiting Current Density of  
906 Vanadium Redox Flow Batteries. *Energies* **2014**, *7*, 5863–5873. doi:<https://doi.org/10.3390/en7095863>.
- 907 69. Gubler, L. Membranes and separators for redox flow batteries. *Current Opinion in Electrochemistry* **2019**,  
908 *18*, 31 – 36. Energy Storage Energy Transformation, doi:<https://doi.org/10.1016/j.coelec.2019.08.007>.
- 909 70. Ke, X.; Alexander, J.I.D.; Prah, J.M.; Savinell, R.F. Flow distribution and maximum current density studies  
910 in redox flow batteries with a single passage of the serpentine flow channel. *Journal of Power Sources* **2014**,  
911 *270*, 646 – 657. doi:<https://doi.org/10.1016/j.jpowsour.2014.07.155>.
- 912 71. Gubler, L. Membranes and separators for redox flow batteries. *Cur. Op. in Elec.* **2019**, *18*, 31–36.  
913 doi:<https://doi.org/10.1016/j.coelec.2019.08.007>.
- 914 72. Prifti, H.; Parasuraman, A.; Winardi, S.; Lim, T.; Skyllas-Kazacos. Membranes for Redox Flow Battery  
915 Applications. *Membranes* **2012**, *2*, 275–306. doi:<https://doi.org/10.3390/membranes2020275>.

- 916 73. Fan, X.; Liu, J.; Yan, C., "Chapter 6: Key Materials of Vanadium Flow Batteries: Membranes" in "Redox  
917 Flow Batteries: Fundamentals and Applications"; 2017; pp. 239–238.
- 918 74. Prifti, H.; Parasuraman, A.; Winardi, S.; Lim, T.; Skyllas-Kazacos, M. Membranes for Redox Flow Battery  
919 Applications. *Membranes* **2012**, *2*, 275–306. doi:10.3390/membranes2020275.
- 920 75. Shi, Y.; Eze, C.; Xiong, B.; He, W.; Zhang, H.; Lim, T.; Ukil, A.; Zhao, J. Recent development of  
921 membrane for vanadium redox flow battery applications: A review. *Applied Energy* **2019**, *238*, 202 –  
922 224. doi:https://doi.org/10.1016/j.apenergy.2018.12.087.
- 923 76. Lim, M.H.; Park, M.J.; Kim, S.C.; Roh, S.; Jung, S.; Kim, H.T.; Jung, H.Y. Chemical Degradation  
924 of Commercial Polymer Electrolyte Membrane for Vanadium Redox Flow Battery (VRFB). *Journal of*  
925 *Nanoscience and Nanotechnology* **2017**, *17*, 5788–5791. doi:10.1166/jnn.2017.14171.
- 926 77. Yuan, X.; Song, C.; Platt, A.; Zhao, N.; Wang, H.; Li, H.; Fatih, K.; Jang, D. A review of all-vanadium redox  
927 flow battery durability: Degradation mechanisms and mitigation strategies. *Int. Journal of Energy Research*  
928 **2019**, pp. 6599–6638. doi:https://doi.org/10.1002/er.4607.
- 929 78. Shi, Y.; Eze, C.; Xiong, B.; He, W.; Zhang, H.; Lim, T.; Ukil, A.; Zhao, J. Recent development of  
930 membrane for vanadium redox flow battery applications: A review. *Applied Energy* **2019**, *238*, 202 –  
931 224. doi:https://doi.org/10.1016/j.apenergy.2018.12.087.
- 932 79. Pisssoort, P.A. FR Patent, 1933.
- 933 80. Pelligri, A.; Spaziante, P.M. GB Patent, 1978.
- 934 81. Rychcik, M.; Skyllas-Kazacos, M. Characteristics of a new all-vanadium redox flow battery. *Journal of*  
935 *Power Sources* **1988**, *22*, 59 – 67. doi:https://doi.org/10.1016/0378-7753(88)80005-3.
- 936 82. Farrow, C. *Uses of Vanadium: Vanadium Redox Flow Battery (VRFB)*, 2019 (accessed May 8, 2020).  
937 doi:http://www.gsa-env.co.uk/news/uses-of-vanadium-vanadium-redox-flow-battery-vrfb/.
- 938 83. Chen, R.; Kim, S.; Chang, Z. Redox Flow Batteries: Fundamentals and Applications **2017**. *2*, 103–118.  
939 doi:https://doi.org/10.5772/intechopen.68752.
- 940 84. Zhong, S.; Skyllas-Kazacos, M. Electrochemical behaviour of vana-dium(v)/vanadium(iv)  
941 redox couple at graphite electrodes. *Journal of Power Sources* **1992**, *39*, 1–9.  
942 doi:https://doi.org/10.1016/0378-7753(92)85001-Q.
- 943 85. Largent, R.; Skyllas-Kazacos, M.; Chieng, J. Improved pv system performance using vanadium  
944 batteries. *Conf. Record of the 23 IEEE Photo-voltaic Specialists Conference* **1993**, *39*, 1119–1124.  
945 doi:https://doi.org/10.1109/PVSC.1993.346967.
- 946 86. Clark, J. *Vanadium*, 2015 (accessed May 9, 2020). doi:https://www.chemguide.co.uk.
- 947 87. Ding, C.; Zhang, H.; Li, X.; Liu, T.; Xing. Vanadium flow battery for energy storage: prospects and  
948 challenges. *J. Phys. Chem. Lett.* **2013**, *13*, 342–345. doi:https://pubs.acs.org/doi/10.1021/jz4001032.
- 949 88. Knehr, K.; Kumbur, E. Open circuit voltage of vanadium redox flow batteries: Discrepancy between models  
950 and experiments. *Electro. Comm.* **2011**, *13*, 342–345. doi:https://doi.org/10.1016/j.elecom.2011.01.020.
- 951 89. Roznyatovskaya, N.; Noack, J.; Mild, H.; Fühl, M.; Fischer, P.; Pinkwart, K.; Tübke, J.; Skyllas-Kazacos, M.  
952 Vanadium Electrolyte for All-Vanadium Redox-Flow Batteries: The Effect of the Counter Ion. *Batteries*  
953 **2019**, *5*. doi:https://doi.org/10.3390/batteries5010013.
- 954 90. Kim, S., *Vanadium Redox Flow Batteries: Electrochemical Engineering*; 2019.  
955 doi:10.5772/intechopen.85166.
- 956 91. Trovò, A.; Picano, F.; Guarnieri, M. Comparison of energy losses in a 9kW vanadium redox flow battery.  
957 *Journal of Power Sources* **2019**, *440*, 227144. doi:https://doi.org/10.1016/j.jpowsour.2019.227144.
- 958 92. Xu, Q.; Ji, Y.; Qin, L.; Leung, P.; Qiao, F.; Li, Y.; Su, H. Evaluation of redox flow batteries goes  
959 beyond round-trip efficiency: A technical review. *Journal of Energy Storage* **2018**, *16*, 108 – 115.  
960 doi:https://doi.org/10.1016/j.est.2018.01.005.
- 961 93. Atkins, P.; L. Jones, C., *Chimie, Molécules, Matière, Métamorphoses*; 1998; Vol. 3.
- 962 94. Service, R. Advances in flow batteries promise cheap backup power. *Science* **2018**, *362*, 508–509.  
963 doi:doi:10.1126/science.362.6414.508.
- 964 95. Buczkowski, T.; Noack, J.; Fischer, P.; Tübke, J.; Pinkwart, K. A Vanadium Redox Flow Battery for  
965 Uninterruptible Power Supply Applications **2015**.
- 966 96. Service, R.F. *New generation of 'flow batteries' could eventually sustain a grid powered by the sun and wind*, 2018  
967 (accessed May 12, 2020).

- 968 97. VanadiumCorp. *Electric Vehicle Applications of Flow Batteries*, 2012 (accessed May 12, 2020).  
969 doi:<https://www.vanadiumcorp.com/news/industry/electric-vehicle-applications-of-flow-batteries-2/>.
- 970 98. Chen, R.; Kim, S.; Chang, Z. Redox Flow Batteries: Fundamentals and Applications **2017**. 2, 103–118.  
971 doi:<https://doi.org/10.5772/intechopen.68752>.
- 972 99. Tokuda, N.; Furuya, M.; Kikuoko, Y.; Tsutui, Y.; Kumamoto, T.; Kanno, T. Development of a redox flow  
973 (RF) battery for energy storage **2002**. 3, 1144–1149. doi:10.1109/PCC.2002.998133.
- 974 100. Group, S.E. *Redox Flow battery*, (accessed May 11, 2020). doi:<https://sei-innovation.com/energy/>.
- 975 101. Kenning, T. *Round-Up: 60MWh Japan project, Northern Ireland's 10MW array and Imergy goes for Africa teleco*,  
976 2015(accessed May 11, 2020).
- 977 102. Fraunhofer-Gesellschaft. *An affordable way to store clean energy*, 2019(accessed May 11, 2020).  
978 doi:<https://www.fraunhofer.de>.
- 979 103. Advanced-Batteries-Energy-Storage-Resources. *China's biggest flow battery project underway*, 2018(accessed  
980 May 11, 2020). doi:<https://www.advancedbatteriesresearch.com>.
- 981 104. Energy-Storage-News. *China's biggest flow battery project so far is underway with hundreds more megawatts to  
982 come*, 2019(accessed May 12, 2020). doi:<https://www.energy-storage.news>.
- 983 105. Soares, R.; Secchi, A. Structural analysis for static and dynamic models. *Mathematical and Computer  
984 Modelling* **2012**, 55, 1051–1067. doi:<https://doi.org/10.1016/j.mcm.2011.09.030>.
- 985 106. Messaggi, M.; Canzi, P.; Mereu, R.; Baricci, A.; Inzoli, F.; Casalegno, A.; Zago, M. Analysis of  
986 flow field design on vanadium redox flow battery performance: Development of 3D computational  
987 fluid dynamic model and experimental validation. *Applied Energy* **2018**, 228, 1057–1070.  
988 doi:<https://doi.org/10.1016/j.apenergy.2018.06.148>.
- 989 107. Yin, C.; Gao, Y.; Xie, G.; Li, T.; Tang, H. Three dimensional multi-physical modeling study of interdigitated  
990 flow field in porous electrode for vanadium redox flow battery. *Journal of Power Sources* **2019**, 438, 227023.  
991 doi:<https://doi.org/10.1016/j.jpowsour.2019.227023>.
- 992 108. Zhang, B.; Lei, Y.; Bai, B.; Xu, A.; Zhao, T. A two-dimensional mathematical model for vanadium redox  
993 flow battery stacks incorporating nonuniform electrolyte distribution in the flow frame. *Applied Thermal  
994 Engineering* **2019**, 151, 495–505. doi:<https://doi.org/10.1016/j.applthermaleng.2019.02.037>.
- 995 109. D'Agostino, R.; Baumann, L.; Damiano, A.; Boggasch, E. A Vanadium-Redox-Flow-Battery Model for  
996 Evaluation of Distributed Storage Implementation in Residential Energy Systems. *IEEE Tran. on Energy  
997 Conv.* **2015**, 30, 421–430. doi:10.1109/TEC.2014.2369437.
- 998 110. COMSOL: *Multiphysics Modeling Software*.
- 999 111. Wang, Q.; Qu, Z.; Jiang, Z.; Yang, W. Numerical study on vanadium redox flow battery performance  
1000 with non-uniformly compressed electrode and serpentine flow field. *Applied Energy* **2018**, 220, 106 – 116.  
1001 doi:<https://doi.org/10.1016/j.apenergy.2018.03.058>.
- 1002 112. Merei, G.; Adler, S.; Magnor, D.; Leuthold, M.; Sauer, D.U. Multi-physics Model for a Vanadium  
1003 Redox Flow Battery. *Energy Procedia* **2014**, 46, 194–203. 8th Int. Ren. Energy Storage Conf. and  
1004 Exh., doi:<https://doi.org/10.1016/j.egypro.2014.01.173>.
- 1005 113. Barton, J.L.; Brushett, F.R. A One-Dimensional Stack Model for Redox Flow Battery Analysis and Operation.  
1006 *Batteries* **2019**, 5. doi:10.3390/batteries5010025.
- 1007 114. Tang, A.; McCann, J.; Bao, J.; Skyllas-Kazacos, M. Investigation of the effect of shunt current on battery  
1008 efficiency and stack temperature in vanadium redox flow battery. *Journal of Power Sources* **2013**, 242, 349 –  
1009 356. doi:<https://doi.org/10.1016/j.jpowsour.2013.05.079>.
- 1010 115. Wei, Z.; Xiong, R.; Lim, T.M.; Meng, S.; Skyllas-Kazacos, M. Online monitoring of state of charge and  
1011 capacity loss for vanadium redox flow battery based on autoregressive exogenous modeling. *Journal of  
1012 Power Sources* **2018**, 402, 252 – 262. doi:<https://doi.org/10.1016/j.jpowsour.2018.09.028>.
- 1013 116. Challapuram, Y.R.; Quintero, G.M.; Bayne, S.B.; Subburaj, A.S.; Harral, M.A. Electrical Equivalent Model  
1014 of Vanadium Redox Flow Battery **2019**. pp. 1–4. doi:10.1109/GreenTech.2019.8767145.
- 1015 117. Han, D.; Yoo, K.; Lee, P.; Kim, S.; Kim, S.; Kim, J. Equivalent Circuit Model Considering Self-discharge for  
1016 SOC Estimation of Vanadium Redox Flow Battery **2018**. pp. 2171–2176. doi:10.23919/ICEMS.2018.8549343.
- 1017 118. Meng, S.; Xiong, B.; Lim, T. Model-Based Condition Monitoring of a Vanadium Redox Flow Battery. **2019**.  
1018 12, 3005. doi:<https://doi.org/10.3390/en12153005>.

- 1019 119. Tang, A.; Bao, J.; Skyllas-Kazacos, M. Thermal modelling of battery configuration and self-discharge  
1020 reactions in vanadium redox flow battery. *Journal of Power Sources* **2012**, *216*, 489–501.  
1021 doi:10.1016/j.jpowsour.2012.06.052.
- 1022 120. Yan, Y.; Skyllas-Kazacos, M.; Bao, J. Effects of battery design, environmental temperature and electrolyte  
1023 flowrate on thermal behaviour of a vanadium redox flow battery in different applications. *Journal of Energy*  
1024 *Storage* **2017**, *11*, 104 – 118. doi:https://doi.org/10.1016/j.est.2017.01.007.
- 1025 121. Yan, Y.; Li, Y.; Skyllas-Kazacos, M.; Bao, J. Modelling and simulation of thermal  
1026 behaviour of vanadium redox flow battery. *Journal of Power Sources* **2016**, *322*, 116 – 128.  
1027 doi:https://doi.org/10.1016/j.jpowsour.2016.05.011.
- 1028 122. Tang, A.; Ting, S.; Bao, J.; Skyllas-Kazacos, M. Thermal modelling and simulation of  
1029 the all-vanadium redox flow battery. *Journal of Power Sources* **2012**, *203*, 165 – 176.  
1030 doi:https://doi.org/10.1016/j.jpowsour.2011.11.079.
- 1031 123. Trovò, A.; Marini, G.; Sutto, A.; Alotto, P.; Giomo, M.; Moro, F.; Guarnieri, M. Standby thermal model  
1032 of a vanadium redox flow battery stack with crossover and shunt-current effects. *Applied Energy* **2019**,  
1033 *240*, 893–906. doi:10.1016/j.apenergy.2019.02.067.
- 1034 124. Wei, Z.; Zhao, J.; Xiong, B. Dynamic electro-thermal modeling of all-vanadium redox flow battery with  
1035 forced cooling strategies. *Applied Energy* **2014**, *135*, 1–10. doi:10.1016/j.apenergy.2014.08.062.
- 1036 125. Shen, H.; Zhu, X.; Cao, H.; Xue, B. Thermal modeling and temperature control of an all-vanadium redox  
1037 flow battery **2019**. pp. 1536–1541.
- 1038 126. Kumar, S.; Jayanti, S. Effect of electrode intrusion on pressure drop and electrochemical  
1039 performance of an all-vanadium redox flow battery. *Journal of Power Sources* **2017**, *360*, 548 – 558.  
1040 doi:https://doi.org/10.1016/j.jpowsour.2017.06.045.
- 1041 127. Tang, A.; Bao, J.; Skyllas-Kazacos, M. Studies on pressure losses and flow rate  
1042 optimization in vanadium redox flow battery. *Journal of Power Sources* **2014**, *248*, 154 – 162.  
1043 doi:https://doi.org/10.1016/j.jpowsour.2013.09.071.
- 1044 128. Xiao, W.; Tan, L. Control strategy optimization of electrolyte flow rate for all vanadium  
1045 redox flow battery with consideration of pump. *Renewable Energy* **2019**, *133*, 1445 – 1454.  
1046 doi:https://doi.org/10.1016/j.renene.2018.09.018.
- 1047 129. Ma, X.; Zhang, H.; Sun, C.; Zou, Y.; Zhang, T. An optimal strategy of electrolyte flow  
1048 rate for vanadium redox flow battery. *Journal of Power Sources* **2012**, *203*, 153 – 158.  
1049 doi:https://doi.org/10.1016/j.jpowsour.2011.11.036.
- 1050 130. Tang, A.; Bao, J.; Skyllas-Kazacos, M. Studies on pressure losses and flow rate  
1051 optimization in vanadium redox flow battery. *Journal of Power Sources* **2014**, *248*, 154 – 162.  
1052 doi:https://doi.org/10.1016/j.jpowsour.2013.09.071.
- 1053 131. Fu, J.; Wang, T.; Wang, X.; Sun, J.; Zheng, M. Dynamic Flow Rate Control for Vanadium Redox Flow  
1054 Batteries. *Energy Procedia* **2017**, *105*, 4482 – 4491. 8th International Conference on Applied Energy,  
1055 ICAE2016, 8-11 October 2016, Beijing, China, doi:https://doi.org/10.1016/j.egypro.2017.03.952.
- 1056 132. Trovò, A.; Picano, F.; Guarnieri, M. Maximizing Vanadium Redox Flow Battery Efficiency: Strategies  
1057 of Flow Rate Control. *2019 IEEE 28th International Symposium on Industrial Electronics (ISIE)* **2019**, pp.  
1058 1977–1982. doi:10.1109/ISIE.2019.8781152.
- 1059 133. Houser, J.; Pezeshki, A.; Clement, J.T.; Aaron, D.; Mench, M.M. Architecture for improved mass  
1060 transport and system performance in redox flow batteries. *Journal of Power Sources* **2017**, *351*, 96 – 105.  
1061 doi:https://doi.org/10.1016/j.jpowsour.2017.03.083.
- 1062 134. Pugach, M.; Parsegov, S.; Gryazina, E.; Bisch, A. Output feedback control of electrolyte  
1063 flow rate for Vanadium Redox Flow Batteries. *Journal of Power Sources* **2020**, *455*, 227916.  
1064 doi:https://doi.org/10.1016/j.jpowsour.2020.227916.
- 1065 135. Bhattacharjee, A.; Saha, H. Development of an efficient thermal management system for Vanadium  
1066 Redox Flow Battery under different charge-discharge conditions. *Applied Energy* **2018**, *230*, 1182 – 1192.  
1067 doi:https://doi.org/10.1016/j.apenergy.2018.09.056.
- 1068 136. Chen, R.; Kim, S.; Chang, Z., Large-scale energy storage. In *Redox Flow Batteries: Fundamentals and*  
1069 *Applications [open access]*; Zhanga, H.; Li, X.; Zhang, J., Eds.; CRC Press, British Columbia, Canada, 2018; pp.  
1070 3–43. doi:10.5772/intechopen.68752.

- 1071 137. Ressel, S.; Bill, F.; Holtz, L.; Janshen, N.; Chica, A.; Flower, T.; Weidlich, C.; Struckmann, T. State of charge  
1072 monitoring of vanadium redox flow batteries using half cell potentials and electrolyte density. *Journal of*  
1073 *Power Sources* **2018**, *378*, 776 – 783. doi:https://doi.org/10.1016/j.jpowsour.2018.01.006.
- 1074 138. Skyllas-Kazacos, M.; Kazacos, M. State of charge monitoring methods for vanadium redox flow battery  
1075 control. *Journal of Power Sources* **2011**, *196*, 8822 – 8827. doi:https://doi.org/10.1016/j.jpowsour.2011.06.080.
- 1076 139. Kroner, I.; Becker, M.; Turek, T. Monitoring the State of Charge of the Positive Electrolyte in a Vanadium  
1077 Redox-Flow Battery with a Novel Amperometric Sensor. *Batteries* **2019**, *5*. doi:10.3390/batteries5010005.
- 1078 140. Xing, Y.; Na, J.; Costa-Castelló, R. Adaptive online parameter estimation algorithm of PEM fuel cells.  
1079 *European Control Conference (CEE)* **2019**, *18*, 441–446. doi:https://doi.org/10.2319/ECC.2019.8795875.
- 1080 141. Ellis, G., Observers in control systems. In *Academic press*; 2002; Vol. 15.  
1081 doi:10.1016/B978-0-12-237472-2.X5000-7.
- 1082 142. Khalil, H., High-Gain observers in nonlinear feedback control. In *Int. Journal of robust and nonlinear control*;  
1083 2013; Vol. 24. doi:10.1002/rnc.2051.
- 1084 143. Xiong, B.; Zhao, J.; Wei, Z.; Skyllas-Kazacos, M. Extended Kalman filter method for state of charge  
1085 estimation of vanadium redox flow battery using thermal-dependent electrical model. *Journal of Power*  
1086 *Sources* **2014**, *262*, 50 – 61. doi:https://doi.org/10.1016/j.jpowsour.2014.03.110.
- 1087 144. Han, D.; Yoo, K.; Lee, P.; Kim, S.; Kim, S.; Kim, J. Equivalent Circuit Model Considering Self-discharge for  
1088 SOC Estimation of Vanadium Redox Flow Battery **2018**. pp. 2171–2176. doi:10.23919/ICEMS.2018.8549343.
- 1089 145. Farahani, S. Chapter 6 - Battery Life Analysis. In *ZigBee Wireless Networks and Transceivers*; Farahani, S., Ed.;  
1090 Newnes: Burlington, 2008; pp. 207 – 224. doi:https://doi.org/10.1016/B978-0-7506-8393-7.00006-6.
- 1091 146. Mohamed, M.; Ahmad, H.; Seman, M.A.; Razali, S.; Najib, M. Electrical circuit model of a vanadium  
1092 redox flow battery using extended Kalman filter. *Journal of Power Sources* **2013**, *239*, 284 – 293.  
1093 doi:https://doi.org/10.1016/j.jpowsour.2013.03.127.
- 1094 147. Xiong, B.; Zhao, J.; Wei, Z.; Skyllas-Kazacos, M. Extended Kalman filter method for state of charge  
1095 estimation of vanadium redox flow battery using thermal-dependent electrical model. *Journal of Power*  
1096 *Sources* **2014**, *262*, 50 – 61. doi:https://doi.org/10.1016/j.jpowsour.2014.03.110.
- 1097 148. Yu, V.; Headley, A.; Chen, D. A Constrained Extended Kalman Filter for State-of-Charge Estimation of a  
1098 Vanadium Redox Flow Battery With Crossover Effects. *ASME. J. Dyn. Sys., Meas., Control.* **2014**, *4*, 136.  
1099 doi:https://doi.org/10.1115/1.4026654.
- 1100 149. Ascencio, P.; Smith, K.; Monroe, C.W.; Howey, D. Adaptive Observer for Charge-State and Crossover  
1101 Estimation in Disproportionation Redox Flow Batteries undergoing Self-Discharge. *2019 American Control*  
1102 *Conference (ACC)* **2019**, pp. 5452–5457. doi:10.23919/ACC.2019.8814764.
- 1103 150. Wei, Z.; Tseng, K.J.; Wai, N.; Lim, T.M.; Skyllas-Kazacos, M. Adaptive estimation of state of charge and  
1104 capacity with online identified battery model for vanadium redox flow battery. *Journal of Power Sources*  
1105 **2016**, *332*, 389 – 398. doi:https://doi.org/10.1016/j.jpowsour.2016.09.123.
- 1106 151. Xiong, B.; Zhang, H.; Deng, X.; Tang, J. State of charge estimation based on sliding mode observer for  
1107 vanadium redox flow battery **2017**. pp. 1–5. doi:10.1109/PESGM.2017.8274042.
- 1108 152. Xiong, B.; Zhao, J.; Su, Y.; Wei, Z.; Skyllas-Kazacos, M. State of Charge Estimation of Vanadium Redox  
1109 Flow Battery Based on Sliding Mode Observer and Dynamic Model Including Capacity Fading Factor.  
1110 *IEEE Transactions on Sustainable Energy* **2017**, *8*, 1658–1667. doi:10.1109/TSTE.2017.2699288.
- 1111 153. Li, X.; Xiong, J.; Tang, A.; Qin, Y.; Liu, J.; Yan, C. Investigation of the use of electrolyte viscosity for online  
1112 state-of-charge monitoring design in vanadium redox flow battery. *Applied Energy* **2018**, *211*, 1050 – 1059.  
1113 doi:https://doi.org/10.1016/j.apenergy.2017.12.009.
- 1114 154. Salkind, A.J.; Fennie, C.; Singh, P.; Atwater, T.; Reisner, D.E. Determination of state-of-charge and  
1115 state-of-health of batteries by fuzzy logic methodology. *Journal of Power Sources* **1999**, *80*, 293 – 300.  
1116 doi:https://doi.org/10.1016/S0378-7753(99)00079-8.
- 1117 155. Álvarez Antón, J.C.; García Nieto, P.J.; Blanco Viejo, C.; Vilán Vilán, J.A. Support Vector Machines  
1118 Used to Estimate the Battery State of Charge. *IEEE Transactions on Power Electronics* **2013**, *28*, 5919–5926.  
1119 doi:10.1109/TPEL.2013.2243918.
- 1120 156. Hansen, T.; Wang, C.J. Support vector based battery state of charge estimator. *Journal of Power Sources* **2005**,  
1121 *141*, 351 – 358. doi:https://doi.org/10.1016/j.jpowsour.2004.09.020.

- 1122 157. Choi, Y.Y.; Kim, S.; Kim, S.; Choi, J.I. Multiple parameter identification using genetic  
1123 algorithm in vanadium redox flow batteries. *Journal of Power Sources* **2020**, *450*, 227684.  
1124 doi:<https://doi.org/10.1016/j.jpowsour.2019.227684>.
- 1125 158. Xiong, B.; Jiyun, Z.; Jinbin, L. Modeling of an all-vanadium redox flow battery and optimization of flow  
1126 rates. 2013, pp. 1–5. doi:10.1109/PESMG.2013.6672599.
- 1127 159. Wei, Z.; Bhattarai, A.; Zou, C.; Meng, S.; Lim, T.M.; Skyllas-Kazacos, M. Real-time monitoring  
1128 of capacity loss for vanadium redox flow battery. *Journal of Power Sources* **2018**, *390*, 261 – 269.  
1129 doi:<https://doi.org/10.1016/j.jpowsour.2018.04.063>.
- 1130 160. Wei, Z.; Xiong, R.; Lim, T.M.; Meng, S.; Skyllas-Kazacos, M. Online monitoring of state of charge and  
1131 capacity loss for vanadium redox flow battery based on autoregressive exogenous modeling. *Journal of*  
1132 *Power Sources* **2018**, *402*, 252 – 262. doi:<https://doi.org/10.1016/j.jpowsour.2018.09.028>.
- 1133 161. Wei, Z.; Meng, S.; Tseng, K.J.; Lim, T.M.; Soong, B.H.; Skyllas-Kazacos, M. An adaptive model for vanadium  
1134 redox flow battery and its application for online peak power estimation. *Journal of Power Sources* **2017**,  
1135 *344*, 195 – 207. doi:<https://doi.org/10.1016/j.jpowsour.2017.01.102>.
- 1136 162. Sun, M.; Su, Y.; Xiong, B.; Zhang, H.; Li, Y. Online Model Identification Method of Vanadium Redox  
1137 Flow Battery Based on Time-varying Forgetting Factor Recursive Least Squares **2019**. pp. 1609–1614.  
1138 doi:10.1109/CAC48633.2019.8996264.
- 1139 163. Chang, Y.; Sun, M.; Jia, W.; Liu, Z. Online Model Identification Method of Vanadium Redox Flow  
1140 Battery Based on Multiple Innovation Recursive Least Squares. *2020 Asia Energy and Electrical Engineering*  
1141 *Symposium (AEEES)* **2020**, pp. 758–762. doi:10.1109/AEEES48850.2020.9121371.
- 1142 164. Wei, Z.; Lim, T.M.; Skyllas-Kazacos, M.; Wai, N.; Tseng, K.J. Online state of charge and model parameter  
1143 co-estimation based on a novel multi-timescale estimator for vanadium redox flow battery. *Applied Energy*  
1144 **2016**, *172*, 169 – 179. doi:<https://doi.org/10.1016/j.apenergy.2016.03.103>.

1145 © 2020 by the authors. Submitted to *Energies* for possible open access publication under the terms and conditions  
1146 of the Creative Commons Attribution (CC BY) license (<http://creativecommons.org/licenses/by/4.0/>).